Arch Appl Mech (2020) 90:1475–1496
https://doi.org/10.1007/s00419-020-01679-2

ORIGINAL

Farzad Vesali · Mohammad Ali Rezvani · Habibolah Molatefi

Simulation of the dynamic interaction of rail vehicle pantograph and catenary through a modal approach

Received: 2 July 2019 / Accepted: 13 February 2020 / Published online: 28 February 2020

Abstract Electric trains rely on the pantograph and the overhead catenary system (OCS) to receive energy from the power main lines. The purpose of this article is to elaborate on the simulation of pantograph and catenary dynamic interaction. The main feature of this method is using a fast analytical approach in order to simulate the entire catenary and to avoid using the finite elements method. This method is making use of the system vibration modes. Therefore, vital phenomenon such as the wave propagation and reflections can also be simulated. Additionally, droppers under compression are simulated as buckled columns that can endure certain amount of compression forces. Inclusion of the proper OCS initial conditions is also a unique add on to this procedure. Evaluation of both static and dynamic responses of catenary is by comparing with the results from some other available software programs. Validation of the results is according to EN 50318: 2002 standard document.

Keywords Rail vehicle dynamic · Catenary · Pantograph · Modal analysis approach · Wave propagation · Dropper slacking

1 Introduction

Overhead catenary systems (OCS) are the most common practice for supplying electricity to electric trains. Provision of continuous connection between pantograph and contact wire with the added necessity for low electrical wear and mechanical wear of collector strip is among the main challenges for engineers and researchers alike regarding the pantograph and catenary interaction. Figure 1 illustrates the railway overhead system and its components [1].

A review of the pantograph and catenary interaction is given in [2]. An attempt to provide pantograph–catenary contact formulations is provided in [3]. A study on the wave, modes and properties with a major impact on the dynamic of pantograph–catenary interaction is provided in [4]. Distributed parameter and finite element models for wave propagation in railway contact lines are provided in [5]. Song et al. have offered an active control of contact force for high-speed railway pantograph–catenary based on multi-body pantograph model [6]. Simulation of the dynamic interaction of pantograph and catenary system is important for predicting the

F. Vesali · M. A. Rezvani (✉) · H. Molatefi
School of Railway Engineering, Iran University of Science and Technology, Tehran 16846-13114, Iran
E-mail: rezvani_ma@iust.ac.ir

F. Vesali
E-mail: vesali@rail.iust.ac.ir

H. Molatefi
E-mail: molatefi@iust.ac.ir

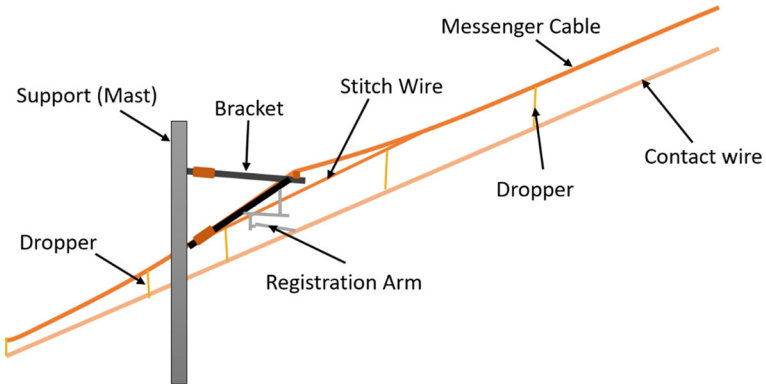

Fig. 1 Schematic of an overhead catenary system

contact force oscillations or contact loss and to improve contact quality. In standard document EN 50367:2012 Claus 7.3, the quality of current collection needs to be proven via simulation or credible test results [1]. In order to simulate the interaction between pantograph and catenary system, several types of engineering software have been developed [7–15]. Most of these software programs use the finite elements method (FEM) to simulate and apply the penalty method for contact between pantograph and contact wire, while in software PrOSA [12] the finite differences method is used for the simulation and integration procedure for the contact model. The most common assumption for such modeling is the idea of lumped masses. Some methods have also succeeded in modeling flexible collector strips as blades, as well.

Based on the analytical procedure that is presented in this research a design software is developed. Contrary to the other available software programs in this field, the theory behind this software is by using the theory of vibration of continuous systems for contact wire, messenger cable and stitch wire in catenary. It means that this procedure does not involve mesh (nor nodes) or elements for the wires. Each mode shape of the wire acts as one degree of freedom. These vibration modes are independent of each other based on the orthogonality of normal modes. In fact, simulation is by finding the modal coordinates of each mode shape.

The description of the contact wire, the messenger cable and that of the stitch wire by a modal synthesis eigenmodes of continuous systems, which are determined analytically, are used as shape functions. The use of these continuous analytical functions saves the effort of the spatial discretization of the structure, which is required for the finite element method. The simulation model, which is implemented in this software, is based on the theory of continuous systems in the sense that it uses analytically determined eigenmodes as shape functions for the modal synthesis. By applying the modal synthesis, the equations of motion are formulated as a system of ordinary differential equations, which can be integrated numerically.

Through this approach it is possible to apply the contact force in the exact position of the contact point (moving load on beams theory), while in FEM approach, all excitation force should be applied on nodes. Another advantage of this approach is its' high accuracy in simulating the wave propagation and reflection.

There are two main reasons for the oscillations in the contact forces including variations in the contact force stiffness and the wave reflections from the boundaries. The vertical stiffness of the catenary means resistance to the vertical deflection in each point of contact wire due to a unique load. Figure 2 is a schematic presentation of the vertical stiffness in a simple catenary and a compound catenary [16].

By increasing the number of the droppers or by using a compound catenary the vertical stiffness of the catenary can become more uniform. Experimental results prove that the contact force in the end of one mechanical section and the beginning of the other mechanical section is practically oscillatory. The oscillations in such overlapping sections in comparison with the other parts in a catenary system are comparably more unstable [14].

In order to reduce such fluctuations in a high-speed catenary system, a higher number of transient (overlapping) sections between the main sections need to be considered. By adding to the number of such overlapping spans, pantograph will not face the reflected waves from its boundaries. Therefore, wave propagation and reflection is as important as stiffness variation in the catenary system and the model needs to consider such effects, as well.

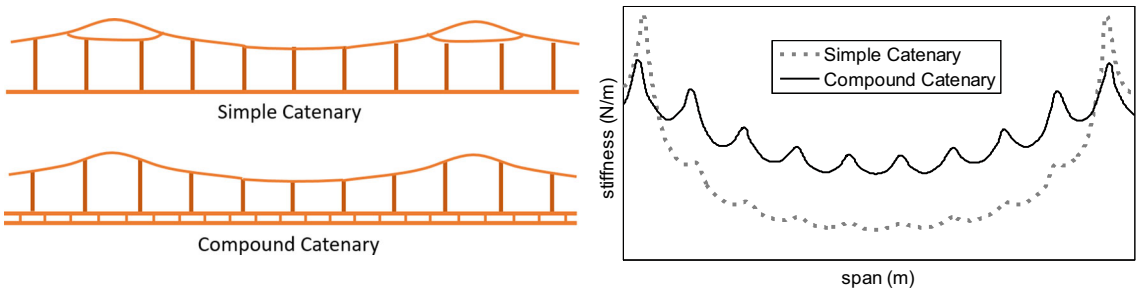

Fig. 2 Vertical stiffness in a simple catenary and a compound catenary [16]

2 Description of the entire model

There are three main methods available for the modeling of the catenary system [16]. The first method, in which the catenary is only represented by a spring with variable stiffness, tries to reproduce the catenary's receptance, i.e., its displacement as a reaction to a force, while the second and the third methods try (at least approximately) to reproduce the catenary's actual structure. Both the second and the third methods consider the wire as a beam; the difference is that the second method, which is a finite element approach, uses a local discretization, i.e., the beam is divided into local sections, in which simple interpolation functions like polynomials are used for describing the wire's displacement field, while in the third method the wire's displacement is described by continuous functions, which are multiplied by scaling factors and superposed.

In the simple model that considers the catenary as a spring with variable stiffness attached to the head of the pantograph the wave propagation cannot be simulated. The second method is based on the Euler–Bernoulli model that is normally used in the FEM approach. The third method is based on a modal analysis approach that decomposes the catenary wire displacement (contact wire, messenger cable and stitch wire) to an infinite derivable sinusoidal functions (mode shapes of the wire) that ensures an infinite continuity. Normally, it is a one-dimensional model where the vertical cable displacement and the flexural wave motion in the wire are taken into account [16].

The model in the present research is based on the analytical model of a tensile Euler–Bernoulli beam. The governing equation for the Euler–Bernoulli beam with the axial force is expressed in Eq. (1).

$$\rho A w_{,tt} + C w_{,t} - T w_{,xx} + E I w_{,xxxx} = F_{\mathrm{g}} + F_{\mathrm{d}}(x) + F_{\mathrm{p}}(t, x), 0 \leq x \leq l, t \geq 0 \tag{1}$$

In this equation, $w(x, t)$ is the beam vertical displacement in time t and space x, ρA is the mass per unit length of beam, C is the beam damping coefficient, T is the axial load applied to the beam (T is positive in tension), and EI is the beam bending stiffness. The gravity load (F_{g}) and the concentrated force exerted on the droppers and the supports (F_{d}) plus the pantograph force $F_{\mathrm{p}}(t, x)$ are also involved on the right side of the equation. For the contact wire the supports are the registration arms, and for the messenger cable, the supports are the masts.

The damping matrix $\mathbf{C}$ and the stiffness matrix $\mathbf{K}$ have an analogous structure. The damping matrix $\mathbf{C}$ can be obtained by simply replacing the stiffness parameters used in the matrix $\mathbf{K}$ by the corresponding damping parameters. There are two effects, which contribute to the stiffness, namely the bending stiffness EI and the axial tension force T. However, only the internal damping of the material contributes to the damping, while there is no damping term analogous to the stiffness due to the axial tension forces.

The essential equation describing the modal synthesis for the wire is presented in Eq. (2). If $\mathbf{q}_k(t)$ is the k-th modal coordinate and $\varphi_k(x)$ is the kth shape function, then the displacement field $W(x, t)$ depending on the location x and on the time t is described by the following equation:

$$w(x, t) = \sum\nolimits_k \varphi_k(x) q_k(t) \tag{2}$$

Applying Eq. (2) to the contact wire, the messenger cable and the stitch wire results in:

$$w_{\mathrm{c}}(x,t)=\sum_{i=1}^{n_{\mathrm{co}}}\mathbf{q}_{\mathrm{ci}}(t)\,\varphi_{\mathrm{ci}}(x)$$
$$w_{\mathrm{m}}(x,t)=\sum_{i=1}^{n_{\mathrm{co}}}\mathbf{q}_{\mathrm{mi}}(t)\,\varphi_{\mathrm{mi}}(x)$$
$$w_{\mathrm{s}}(x,t)=\sum_{i=1}^{n_{\mathrm{co}}}\mathbf{q}_{\mathrm{si}}(t)\,\varphi_{\mathrm{si}}(x) \tag{3}$$

where w_{c}, w_{m}, w_{s} represent the displacements for the contact wire, the messenger cable and the stitch wire, respectively. $\mathbf{q}_{\mathrm{ci}}$, $\mathbf{q}_{\mathrm{mi}}$, $\mathbf{q}_{\mathrm{si}}$ represent the modal coordinates for the contact wire, the messenger cable and the stitch wire, respectively. $\varphi_{\mathrm{ci}}(x)$, $\varphi_{\mathrm{mi}}(x)$, $\varphi_{\mathrm{si}}(x)$ represent the mode shapes for the contact wire, the messenger cable and the stitch wire, respectively. n_{co} is the natural frequency that needs to be more than the maximum amount for the cutoff frequency of the case of study.

For the contact wire, the messenger cable and the stitch wire by replacing the terms from Eq. (3) into Eq. (1) and by considering the following clamp–clamp boundary conditions the natural frequencies (the eigenvalues) and the mode shapes (the eigenvectors) for each case are obtainable.

$$\begin{cases} w(0,t)=0,\ \mathrm{d}w/\mathrm{d}x\,(0,t)=0 \\ w(l,t)=0,\ \mathrm{d}w/\mathrm{d}x\,(l,t)=0 \end{cases} \tag{4}$$

$w(x,t)$ is the displacement in position x at time t. The boundary conditions that are presented in Eq. (4) are the same for the contact wire, the messenger cable and the stitch wire.

Since the modeling for the wires and cables in this study is based on the tensile Euler–Bernoulli beam, the following corresponding mode shapes need to be considered [17].

$$\varphi(x)=C_1\mathrm{Sin}\,\alpha_1 x+C_2\mathrm{Cos}\,\alpha_1 x+C_3\mathrm{Sinh}\,\alpha_2 x+C_4\mathrm{Cosh}\,\alpha_2 x \tag{5}$$
$$\alpha_{1,2}^2=\mp\frac{T}{2EI}+\sqrt{\left(\frac{T}{2EI}\right)^2+\frac{\rho A\omega^2}{EI}} \tag{6}$$

In Eq. (6) T is the tension in cable, EI is the bending stiffness, ρA is the mass per unit length, and ω is the cable natural frequency.

Each of the boundary conditions in Eq. (4) results in a set of equations that in matrix form can be presented as in Eq. (7).

$$\mathbf{F}\emptyset=\begin{bmatrix} f_{11} & f_{12} & f_{13} & f_{14} \\ f_{21} & f_{21} & f_{21} & f_{21} \\ f_{31} & f_{32} & f_{33} & f_{34} \\ f_{41} & f_{42} & f_{43} & f_{44} \end{bmatrix},\quad \mathbf{F}\emptyset\begin{bmatrix} C_1 \\ C_2 \\ C_3 \\ C_4 \end{bmatrix}=\begin{bmatrix} 0 \\ 0 \\ 0 \\ 0 \end{bmatrix} \tag{7}$$

where f_{ij} represents the term accompanying the coefficient C_j at boundary condition i. As examples $f_{11}=\mathrm{Sin}\,\alpha_1(x=0)=0$ & $f_{33}=\mathrm{Sinh}\,\alpha_2(x=l)=\mathrm{Sinh}\,\alpha_2 l$.

Setting the characteristic polynomial of matrix $\mathbf{F}\emptyset$ equal to zero results in its eigenvalues. The resulting eigenvalues are the natural frequencies (ω) of the wire/cable. It is then possible to obtain the corresponding mode shapes (eigenvectors) by using Eq. (5). At this stage the process of modal analysis for each of the wires in the catenary system is accomplished.

In order to obtain the forced vibration response of the system initially Eq. (2) needs to be replaced in Eq. (1) for each of the wires. Then both sides of this equation need to be multiplied by the i-th mode shape ($\varphi_j(x)$) that results in Eq. (8)

$$\varphi_j(x)\left(\rho A\sum\nolimits_{i=1}^{n_{\mathrm{co}}}\ddot{\mathbf{q}}_i(t)\,\varphi_i(x)+C\sum\nolimits_{i=1}^{n_{\mathrm{co}}}\dot{\mathbf{q}}_i(t)\,\varphi_i(x)-T\sum\nolimits_{i=1}^{n_{\mathrm{co}}}\mathbf{q}_i(t)\,\varphi_i''(x)\right.$$
$$\left.+EI\sum\nolimits_{i=1}^{n_{\mathrm{co}}}\mathbf{q}_i(t)\,\varphi_i^{(4)}(x)\right)=\varphi_j(x)\left(F_{\mathrm{g}}+F_{\mathrm{d}}(x)+F_{\mathrm{p}}(t,x)\right), \tag{8}$$

Since the clamp–clamp boundary conditions are considered, the principal of the orthogonality of the mode shapes can be used that ends up with the ordinary differential equations.

By using the method of the separation of variables and by considering the proper boundary conditions, the modal analysis of the beam can be accomplished and the natural frequencies and mode shapes of the beam can be extracted. Expansion of the eigenfunctions can be used in order to change the partial equations of a tensile beam to a system of ordinary deferential equation as in Eq. (1).

Furthermore, in order to obtain the equations of motion for each modal coordinate $\mathbf{q}_i(t)$ the sum describing the modal synthesis is inserted into partial differential equation (1) and afterward the partial differential equation is multiplied by the i-th shape function $\varphi_i(x)$ and integrated over the entire length l of the wire.

$$\int_0^l \varphi_i(x)\left(\rho A\frac{\partial^2 w}{\partial t^2}+C\frac{\partial w}{\partial t}-T\frac{\partial^2 w}{\partial x^2}+EI\frac{\partial^4 w}{\partial x^4}-F_{\mathrm{g}}-F_{\mathrm{d}}(x)\right)\mathrm{d}x=0 \tag{9}$$

The same modeling approach is also used for both the contact wire and the messenger cable. However, both wires are not exactly straight: The contact wire is installed in a lateral zigzag, and the messenger cable clearly shows the catenary shape between two supports as shown in Fig. 2. However, these deviations from the ideal straight shape have only a weak impact on the mechanical behavior so that these effects may be neglected. Furthermore, it needs to be mentioned that besides the gravitational force and the dropper force the contact wire is also subject to the pantograph force; therefore, the term $F_{\mathrm{d}}(x)$ can also be interpreted as "discrete forces," which include the dropper forces and the pantograph force with the difference that for the dropper force the location indicated by x is constant, while for the moving pantograph force x is varying. Though not used, it is also reasonable to introduce a sum $\sum F_{\mathrm{d,I}}(x)$ in order to underline that there are several discrete forces acting on the messenger cable and on the contact wire.

For the evaluation of the integral the orthogonality of the shape functions is used. Shape functions of the following form are used:

$$\varphi_k(x)=\sin\left(\frac{2\pi k}{l}x\right),\ k\in N \tag{10}$$

The orthogonality of the shape functions is an important property, which leads to the relatively simple form of the equations of motion according to Eq. (2). The orthogonality relation can be formulated in the following manner:

$$i,k\in N,\ i\neq k:\ \int_0^l \varphi_i(x)\varphi_k(x)\mathrm{d}x=\int_0^l \sin\left(\frac{2\pi i}{l}x\right)\sin\left(\frac{2\pi k}{l}x\right)\mathrm{d}x=0 \tag{11}$$

$$\ddot{q_i}(t)+c\dot{q_i}(t)+\omega_i^2 q_i(t)=\alpha_n\int_0^l \varphi_i(x)(F_{\mathrm{g}}+F_{\mathrm{d}}(x))\mathrm{d}x,\ t>0$$

$$\alpha_n=\frac{1}{\rho A\int_0^l \varphi_i^2(x)\,\mathrm{d}x} \tag{12}$$

In Eq. (12), $q_i(t)$ is the modal coordinates and $\varphi_i(x)$ is the spatial term or the mode shape function of the ith mode shape. If the excitation forces on the right side of Eq. (12) are caused by a spring, damper or mass, they will shift to the left side of the equation and add to coefficients of $q_i(t)$, $\dot{q_i}(t)$ and $\ddot{q_i}(t)$. Therefore, an equation of a tensile beam with an attached lamped mass, or a spring or a damper and with any concentrated or distributed forces can be expressed in the form of the following matrix equation (Eq. 13).

$$\mathbf{M}\ddot{\boldsymbol{x}}+\mathbf{C}\dot{\boldsymbol{x}}+\mathbf{K}\boldsymbol{x}=\mathbf{B}\mathbf{u} \tag{13}$$

In Eq. (13) **M** is the mass matrix, **C** is the damping matrix, **K** is the stiffness matrix, and **Bu** is the excitation vector. The details of each matrix are provided in "Appendix A."

3 The modeling procedure

The method of solution in this research has become the basis for developing a software that from hereon is called CatAna (brief for the Catenary Analysis). The modeling also includes the following procedures:

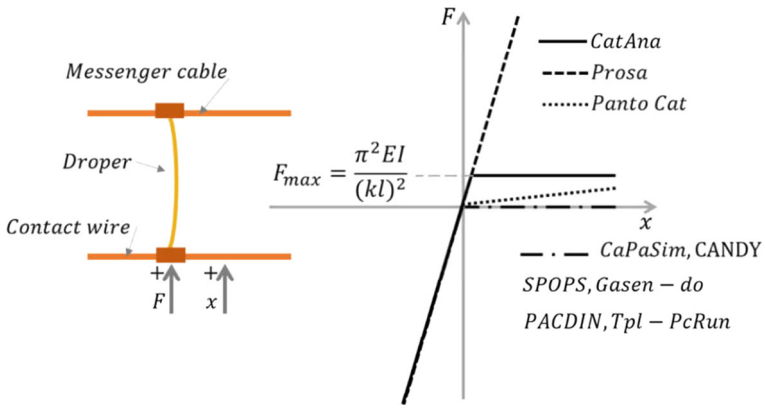

Fig. 3 A collection of methods with different assumptions for the dropper stiffness

3.1 Droppers and slacking

All elements within a catenary system can be considered as behaving linearly except its droppers. Catenary droppers exhibit high stiffness in tension but buckle easily in compression; hence, they cannot be modeled as a linear spring. Some methods of solution that have become publically available in this field, even in the form of engineering software, are based on the assumption that catenary droppers cannot transmit any compressive forces. The evidence is that catenary droppers buckle under compression and thereby cannot transmit compressive forces. In some other methods stiffness of the dropper in compression is less than that in tension [15]. In two engineering software programs introduced as PrOSA [12] and TPL-PCRUN [18], catenary droppers are modeled as linear springs both in compression and in tension.

It is clear that catenary droppers can endure degrees of compressive loads. Thus, in this research the method of solution considers droppers as linear springs, while in tension and if in compression it is also a linear component up to its limit for buckling. The limit for buckling for each dropper depends on its length. A comparison between selections of assumptions for the catenary dropper stiffness is provided in Fig. 3. In Fig. 3, $F_{\max}$ is the buckling force plus the static force (or the dead load) of each dropper. The names PrOSA, PantoCat, CaPaSIM, CANDY, SPOPS, Gasen-do, PACDIN, TPL-PCRUN that are used in Fig. 3 refer to the various software programs that are developed by different researchers for the estimations of the catenary–pantograph dynamic interactions. These are also referred to later on in this article.

3.2 Registration arm model

A registration arm connects the contact wire to its supports (Fig. 1) and creates a zigzag in the contact wire. Registration arm is hinged to the support, and the arm does not have vertical stiffness on its own. However, because of the changing of the orientation of tension in the contact wire, pantograph can sense vertical stiffness under the registration arm. The zigzag in the contact wire that is caused by the registration arm and its vertical stiffness is illustrated in Fig. 4.

The magnitude of the registration arm stiffness (K_{re}) is dependent on T the tension in the contact wire, d_{st} the stager distance, l_{re} the length of the registration arm and l_{sp} the span length. It can be calculated according to Eq. (14).

$$K_{\text{re}} = 2T\left(\frac{d_{\text{st}}}{l_{\text{re}} l_{\text{sp}}} + \frac{1}{l_{\text{sp}}}\right) \tag{14}$$

Additionally, an equivalent lumped mass needs to be considered that represents the registration arm in the model. If a uniform distribution of mass for the registration arm is considered, the equivalent mass is then $1/3m_{\text{re}}$, which m_{re} is the total mass of the registration arm.

3.3 Stitch wire model

Stitch wires are used in some types of catenaries. It helps in producing a uniform distribution of the vertical stiffness in the contact wire. For the analytical modeling, the stitch wire can be modeled as a tensile Euler–

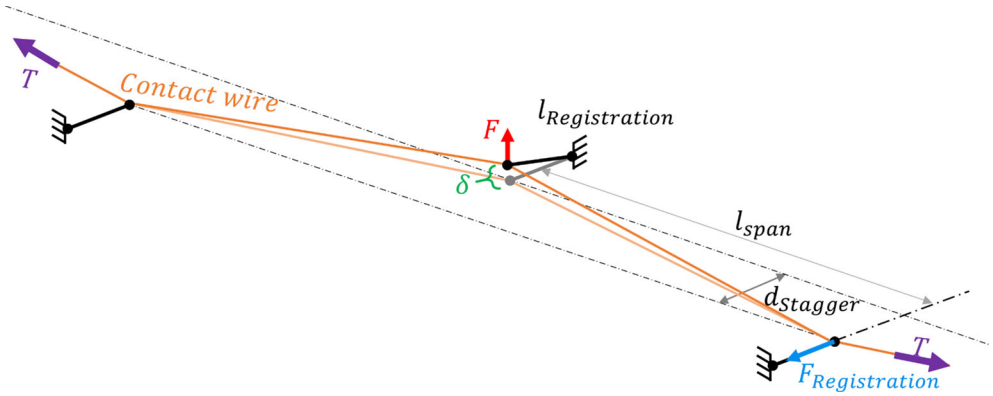

Fig. 4 The vertical stiffness of the registration arm and the zigzag in the contact wire

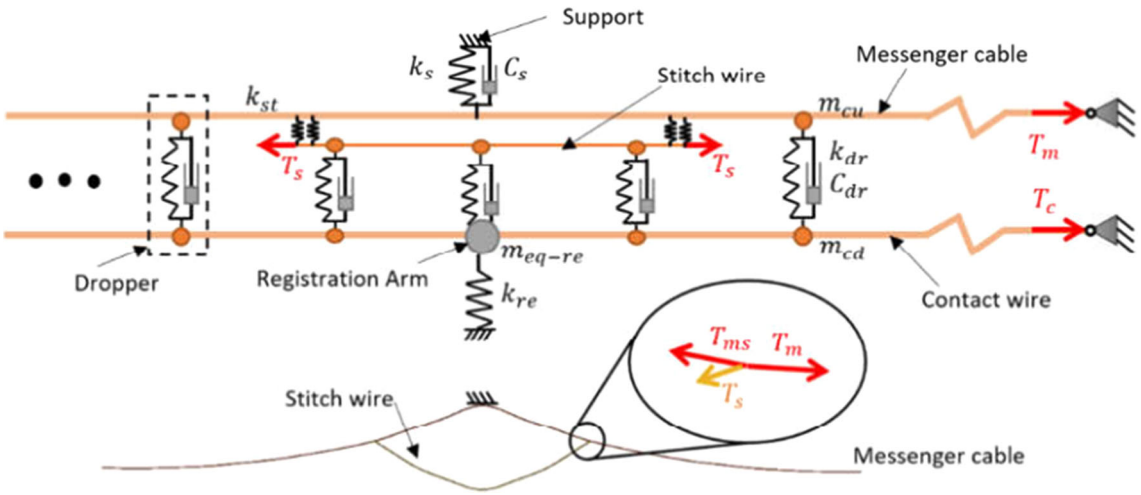

Fig. 5 The model for a stitch wire highlighting the tension in the messenger cable and in the stitch wire

Bernoulli beam, the same as the contact wire or the messenger cable, Fig. 5. The mathematical description of the eigenmodes for the stitch wire is presented in Eq. (3). The number of the modes considered depends on the length of the spans, number of spans and tension in spans. Since the ends of the stitch wire, where it is connected to the messenger cable, must be able to move, the modeling is based on the method that is presented in [19]. This is by adding two degrees of translational and rotational freedoms for the wire with the corresponding modal coordinates. By using this method movements of the two ends of the stitch wire are also included. In this model the messenger cable and the stitch wire are connected to each other via two stiff springs. The tension in stitch wire is adjusted according to the stitch wire tension in the catenary. However, practically in a catenary the part of the messenger cable that is located over the stitch wire has less tension compared with the other part of the messenger cable ($T_s + T_{ms} = T_m$). For the ease of the simulation in this research, tension in all messenger cable is considered as constant ($T_{ms} = T_m$). A reasonable justification is that in an analytical procedure inclusion of two different tensions in two different sections of the wire is not possible.

Since the magnitude of tension in the stitch wire is less than 0.2% in the messenger cable and the wave in the messenger cable is not as important as in the contact wire, this parameter cannot create a significant error in the results.

The parameters that are used for the simulation are presented in Table 1.

3.4 Pantograph model

Two widely used methods for pantograph modeling are reported by Kia et al. [16]. These include the low-order pantograph model that considers two or three concentrated masses that connect to each other by linear springs

Table 1 The parameters for the simulation

Parameter	Description	Parameter	Description
Catenary			
k_{st}	Stiffness of stitch wire and messenger cable connection	$\mathbf{m}_{eq-re}$	Equivalent mass of registration arm
$\mathbf{k}_s$	Stiffness of support (Mast)	T_s	Tension of stitch wire
$\boldsymbol{c}_s$	Damping of support (Mast)	$\mathbf{m}_{cu}$	Mass of upper clamp of dropper
$\mathbf{k}_{dr}$	Stiffness of dropper	$\mathbf{c}_{dr}$	Damping of dropper
$\mathbf{m}_{cd}$	Mass of lower clamp of dropper	T_m	Tension of messenger cable
T_c	Tension of contact wire	T_{ms}	Tension on messenger cable over stitch wire
		$\mathbf{k}_{re}$	Equivalent stiffness of registration arm
Pantograph			
		K_c	Stiffness of contact point
m_{p1}, m_{p2}	Masses of pantograph parts	k_{p1}, k_{p2}	Stiffness of pantograph parts
C_{p1}, C_{p2}	Damping of pantograph parts	y_1, y_2	Vertical movement of pantograph parts
F_u	Uplift force	V_p	Pantograph speed

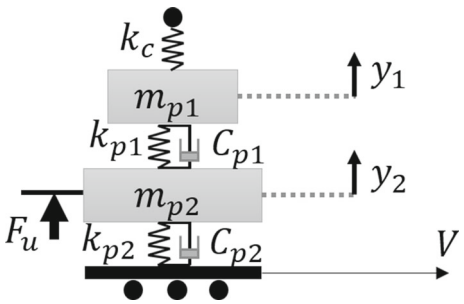

Fig. 6 The model for a pantograph

and dampers and the multibody method that models the rigid elements of the pantograph by considering their geometry and dynamic properties.

In this research, based on the recommendation in EN50318, pantograph is modeled as two lumped masses with a linear spring and viscous damping connection. Uplift force is applied to the lower mass of the pantograph (m_{p2} in Fig. 6). Since m_{p2} is connected to the roof of the car body by a spring (k_{p2} in Fig. 6), the mean value of the contact force will be less than the uplift force.

3.5 Model of the pantograph–catenary contact

Since the analytical model of a tensile beam is considered for the contact wire, the penalty method is used for the modeling of the pantograph and catenary contact. This is exactly based on the assumption of a linear spring with the added assumption that while in tension the force will not change direction and will stay null. In fact the contact point is assumed as a spring with a stiffness of 50 kN/m (k_c in Fig. 6). As long as the contact force is positive, the results are valid. Equation (15) describes the pantograph and catenary contact model.

$$F_c = k_c \left(y_1 - w_c \left(V_p t, t\right)\right) \qquad w_c \left(V_p t, t\right) = \sum_{i=1}^{n_{co}} q_i \left(t\right) \varphi_i \left(V_p t\right) \tag{15}$$

where $w_c\left(x, t\right)$ is the deflection of the contact wire that is a function of the location on the contact wire and the time. $V_p t$ is the location of the contact point on the contact wire. $\varphi_i \left(V_p t\right)$ is the ith mode shape (eigenfunction) of the contact wire, and $q_i\left(t\right)$ is a modal coordinate for each mode shape. n_{co} is the cutoff frequency. The number n_{co} is chosen in such a way that all eigenmodes belonging to eigenfrequencies up to 60 Hz are used as shape functions.

4 Structure of the simulation model

The analytical procedure for the simulation of the dynamic interaction between the pantograph and catenary through a modal approach that is elaborated on in the prior sections of this report is put together to produce

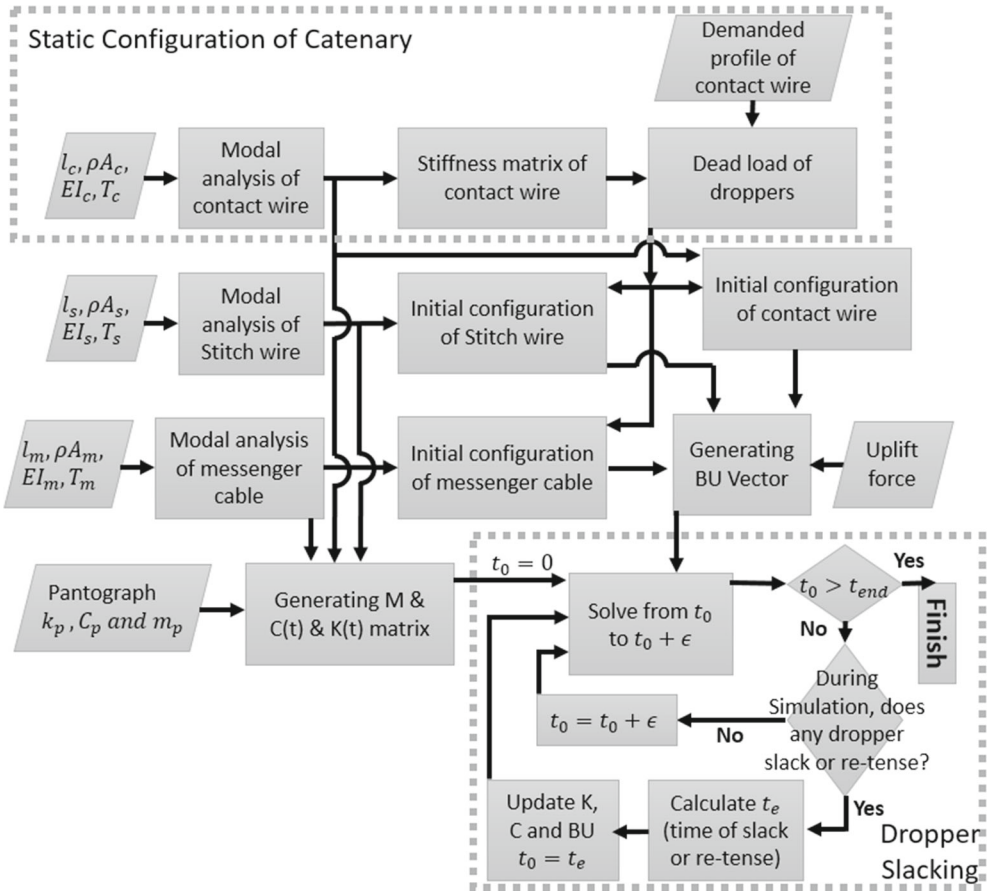

Fig. 7 The simulation flowchart

a software that can be used for practical purposes. This software from hereon is called CatAna (brief for the Catenary Analysis). The flow of actions in this software is presented in Fig. 7. A sample output from the software CatAna is presented in Fig. 8.

The program output window includes five subwindows. Subwindow A at the top animates the vertical deflection of the whole mechanical section and the position of the pantograph. Subwindow E at the bottom is similar to Subwindow A, but instead of the vertical deflection, the vertical acceleration is animated. The vertical acceleration is useful for sensing the effect of the wave reflection in the contact wire on the contact force oscillation. Subwindows B and C at the middle and the left side of the screen produce zoomed windows to the pantograph deflection and acceleration, respectively. The zooming action is useful to observe the effect of the location of the droppers on the maximum and the minimum states of the contact force. Subwindow D in the middle of the right corner of the screen presents a time history of the contact force. There are also many other useful data such as the contact force and the vertical deflection of the contact point that can be accessed for further processing.

5 The numerical integration procedure

Each mode shape of the contact wire and the messenger cable is considered as a degree of freedom for the dynamic system. Therefore, the dimension of the stiffness, mass and damping matrices of the system (**K**, **M** and **C**) can be calculated by using the following Eq. (16).

$$n_{\mathrm{sy}} = n_{\mathrm{co}} + n_{\mathrm{ms}} + n_{\mathrm{st}} + n_{\mathrm{pa}} + n_{\mathrm{ex}} \tag{16}$$

n_{sy} is the dimension of the whole system. $n_{\mathrm{co}}, n_{\mathrm{ms}}, n_{\mathrm{st}}$ represent the number of shape function that are to be considered for the contact wire, the messenger cable and the stitch wire, respectively. In fact, $n_{\mathrm{co}}, n_{\mathrm{ms}}, n_{\mathrm{st}}$ are the numbers of the shape functions, which are taken into account in the modal synthesis for each component,

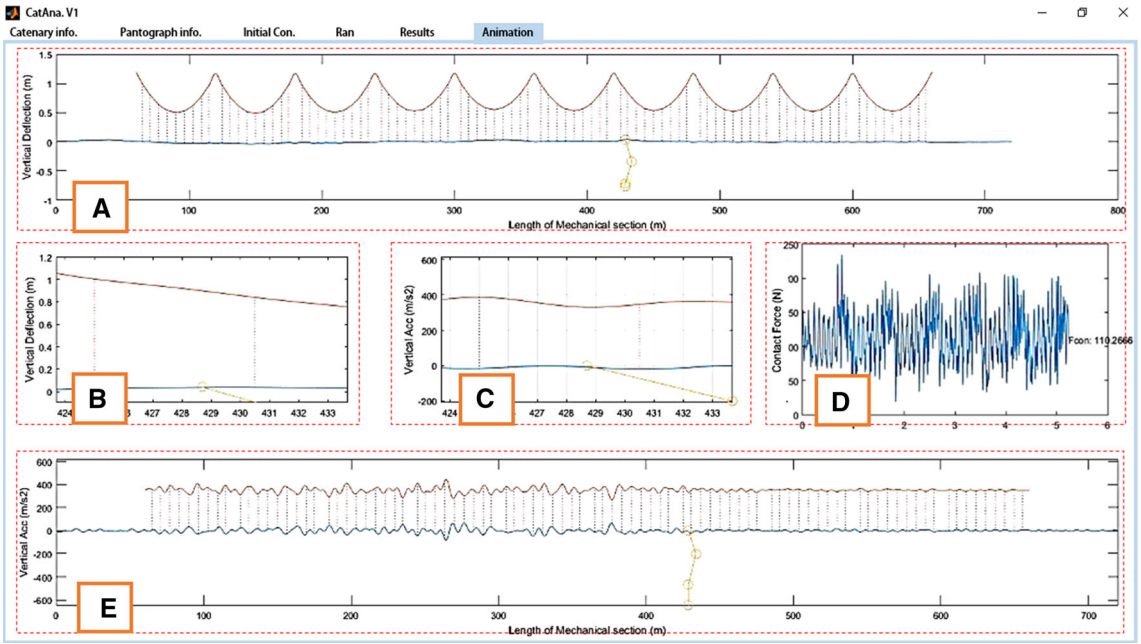

Fig. 8 A sample output from the simulation program CatAna

and since each shape function $\varphi_k(x)$ is scaled by a corresponding modal coordinate $q_k(t)$, which is a degree of freedom, the numbers, n_{co}, n_{ms}, n_{st} also indicate the total number of degrees of freedom. Of course, the number of the shape functions used in the modal synthesis depends on the limit for the corresponding eigenfrequencies, but it also depends on the properties of the structure itself, in particular its length. In other words, the longer the structure is, the more eigenfrequencies are obtained below a certain limit. n_{pa} is the pantograph(s) degrees of freedom. $n_{pa} = 2$ in case of using one pantograph and $n_{pa} = 4$ in case of using 2 pantographs. n_{ex} represents the additional objects that may need to be added to the model, such as a tuned mass damper. The contact point of the pantograph and the stiffness and damping of the droppers are time-dependent variables. Therefore, the stiffness and damping of the whole system is time dependent, as well.

The governing differential equation of the whole pantograph–catenary system can be expressed in the form of state space equations, Eq. (17);

$$\begin{aligned}
&\mathbf{M}\ddot{\mathbf{q}}(t) + \mathbf{C}(t)\dot{\mathbf{q}}(t) + \mathbf{K}(t)\mathbf{q}(t) = \mathbf{B}(t)\mathbf{u} \\
&\ddot{\mathbf{q}}(t) = \mathbf{M}^{-1}\mathbf{C}(t)\dot{\mathbf{q}}(t) + \mathbf{M}^{-1}\mathbf{K}(t)\mathbf{q}(t) + \mathbf{M}^{-1}\mathbf{B}(t)\mathbf{u} \\
&\begin{bmatrix} \dot{\mathbf{q}}(t) \\ \ddot{\mathbf{q}}(t) \end{bmatrix} = \begin{bmatrix} \mathbf{0} & \mathbf{I} \\ \mathbf{M}^{-1}\mathbf{K}(t) & \mathbf{M}^{-1}\mathbf{C}(t) \end{bmatrix} \begin{bmatrix} \mathbf{q}(t) \\ \dot{\mathbf{q}}(t) \end{bmatrix} + \begin{bmatrix} \mathbf{0} \\ \mathbf{M}^{-1}\mathbf{B}(t)\mathbf{u} \end{bmatrix}
\end{aligned} \tag{17}$$

$\mathbf{K}(t)$, $\mathbf{M}$ and $\mathbf{C}(t)$ are the stiffness, mass and damping matrices of the whole system, respectively. $\bar{q}$ is a vector that includes the modal coordinates of the mode shapes of the contact wire, messenger cable, stitch wire and pantograph(s). $\mathbf{B}(t)\mathbf{u}$ contains all input forces such as the gravity forces, the dropper dead loads and the uplift forces of the pantograph(s). Since the state space system of Eq. (17) is a nonstiff medium-order equation, it is solved by using ODE 45 solver in MATLAB engineering software that is based on an explicit Runge–Kutta method [20].

It needs to be reminded that U represents a constant that does not vary with time. The process for acquiring U is made available in the section for "Appendix." The dynamic of the system is not due to the variations at the system entry. Rather it is caused by the variation of the system stiffness with time. Variations of the system stiffness with time are also caused by the movements of the pantograph and the appearance and the disappearance of the droppers' stiffness. While the system is described by linear equations, the nonlinear behavior of the droppers at any instant is linearized.

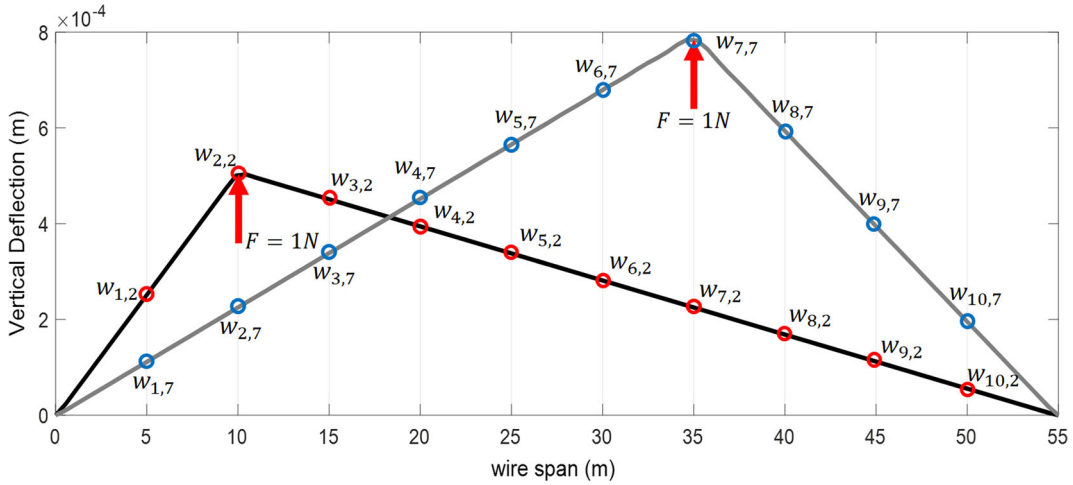

Fig. 9 Measuring deflections of dropper points after applying unique forces in dropper locations, in order to calculate the stiffness matrix of the contact wire

6 Solver initialization (steady-state configuration of the catenary)

The steady-state configuration of the catenary is significant in practice and in modeling. The positioning of the contact wire is vital since it is in direct contact with the pantograph. In some catenaries a pre-sag is used to provide a uniform stiffness gradient for the contact wire. However, in some recent applications the contact wire profile is designed without the sag. For a proper simulation the simulated contact wire profile and its initial conditions need to be as close to the real case scenario as possible.

In practice, for catenary installation some equipment and tools are used to adjust the length of the droppers and to form the contact wire profile. For the purpose of modeling the catenary the static load or the dead load of the droppers should be calculated in such a way that the contact wire finds its' demanded profile. Hence, for the initialization of the problem in a catenary model the required force for each dropper should be calculated.

The analytical procedure that is offered in this research makes it possible to accurately calculate the droppers' static load, hence providing a proper profile for the contact wire. This is a major advantage of the analytical solution procedure over the methods that are based on the finite elements method.

The method of solution that is presented in this research provides exact results for the dropper's dead loads based on the analytical procedure that was introduced in [21]. Initially, the method finds the stiffness matrix for the whole length of the contact wire according to its length, density, bending stiffness and tension. The unique static load is applied at the droppers' locations, and the resulting deflection at such locations determines the stiffness matrix of the contact wire. This procedure is schematically presented in Fig. 9.

The arrays of the corresponding stiffness matrix are presented in Eq. (18).

$$\mathbf{K}_{\text{con}} = \begin{bmatrix} w_{1,1} & w_{1,2} & \cdots & w_{1,3} \\ w_{2,1} & w_{2,2} & \cdots & \vdots \\ \vdots & \vdots & \ddots & \vdots \\ w_{nd,1} & w_{nd,2} & \cdots & w_{nd,nd} \end{bmatrix}^{-1} \tag{18}$$

$\mathbf{K}_{\text{con}}$ is the stiffness matrix of the contact wire, n_{d} is the number of the droppers in the mechanical section, $w_{i,j}$ is the contact wire deflection in location of the ith dropper that is resulted by applying a unique force in location of the jth dropper.

When the stiffness matrix is calculated, it is then needed to find the required force vector to fit the contact wire in its demanded profile. To start with, the profile of the contact wire due to its weight ought to be calculated. Then the stiffness matrix is multiplied by the difference between the demanded profile and the weight profile of the contact wire (Eq. 19).

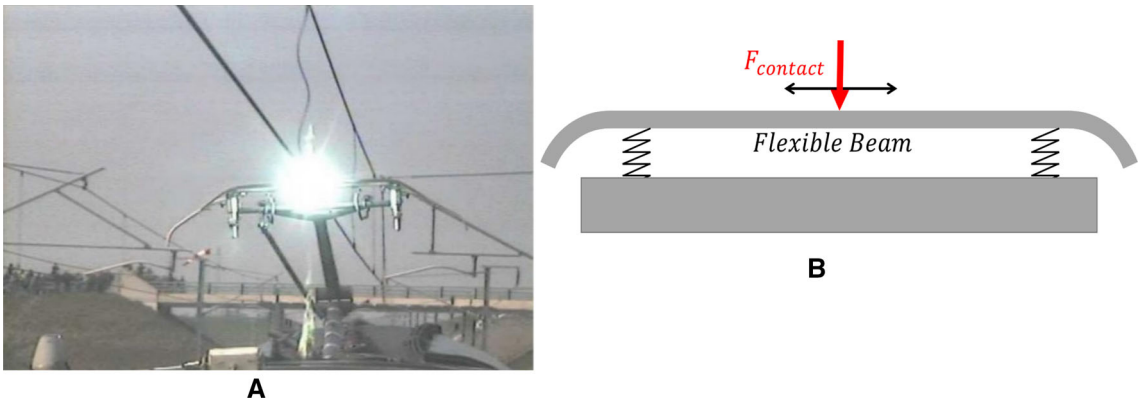

Fig. 10 a Impulse loading of droppers by passing high-speed pantograph and buckling of dropper in the 3rd mode [22]. **b** Modeling collector strip as flexible beam with moving load

$$\mathbf{f}_{\mathrm{dr}} = \mathbf{K}_{\mathrm{con}} \times \begin{bmatrix} y_{\mathrm{de}}\,(x = x_1) - y_g\,(x = x_1) \\ y_{\mathrm{de}}\,(x = x_2) - y_g\,(x = x_2) \\ \vdots \\ y_{\mathrm{de}}\,(x = x_{\mathrm{ndr}}) - y_{\mathrm{g}}\,(x = x_{\mathrm{ndr}}) \end{bmatrix} \tag{19}$$

where $y_{\mathrm{de}}(x)$ is the function of the demanded profile of the contact wire (in most catenary designs it is equal to zero), $y_{\mathrm{g}}(x)$ is a function of the contact wire profile due to the weight, $\mathbf{K}_{\mathrm{con}}$ is the stiffness matrix of the contact wire, and $\mathbf{f}_{\mathrm{dr}}$ is the static force of the dropper that is needed to fit the contact wire in its demanded profile. The steady-state configuration of the contact wire can be obtained by applying these dead loads to the contact wire in the upward direction and to the messenger cable in the downward direction. At this stage, the initial length of the droppers can be calculated according to the initial profiles of the messenger cable and the contact wire.

7 Comments for further modeling steps

One of main advantages of the method of solution that is developed in this research is to provide an accurate model of the functioning of the droppers that also considers buckling under compression. This is unique and has not been reported in the corresponding literature.

The buckling force is a function of the length of the object. Therefore, the shorter droppers can endure more compressive forces. In addition, it seems that the droppers in high-speed crossings of the pantograph tend to buckle in their higher modes of buckling (2nd, 3rd, …). In Fig. 10a it is revealed that a dropper buckles in its 3rd mode, while a high-speed pantograph is passing underneath it [22].

When a load is applied to a column as a single pulse of amplitude that is much higher than the static buckling load of the column a certain type of dynamic buckling or the so-called pulse buckling happens [23]. In dynamic buckling the critical buckling force exceeds the Euler force even at a relatively slow compression rate [24]. Therefore, in a high-speed pantograph crossing, the maximum force from the pantograph is more than the Euler force. The maximum enduring force of the droppers' is calculated as a function of the length of the droppers and the speed of the pantograph.

It is also possible to model the collector strip of the pantograph as a beam with suspended support. This beam gets excited by the contact force that acts as a moving load (Fig. 10b). Any additional damper can be added to the model, as well. The self-damping of the messenger cable can be increased and tuned mass dampers (TMD) or beam dampers can be added to both the messenger cable and the contact wire.

8 Further modeling concerns, wave propagation and reflection

8.1 The suspended support

In a real contact wire of the catenary system there is no vertical support to restrain the vertical motion of the cable in each mechanical section. Tension in the contact wire is provided by auto-tension devices in each mechanical section.

Therefore, in case of real contact wires, there is no wave reflection. In order to omit the wave reflection in the results, the boundary condition needed to be changed from clamp–clamp to the suspended support. The suspended support is used in several FEM-based studies [25]. The spring–damper support is not a conventional boundary condition, and orthogonality of mode shapes is not confirmed. In this approach initially modal analysis of a beam with the free-free boundary conditions is performed. Then two more degrees of freedom including the rigid rotation and the rigid displacement are added to its mode shapes. Therefore, in what follows, this method is used to solve for a case with suspended supports.

9 The lengthy span

An alternative approach to omit the wave reflection error in the results is by considering longer cables in such a way that the reflected wave does not get a chance to appear within the span of consideration. In other words, by considering a lengthy span, the wave exits the span of interest with no chance for reflection. The gravity force is applied only to the span of interest, and the moving load starts its motion from the beginning of that span.

The number of the considered natural frequencies for the lengthy span should be more than the simple span in order to observe the same wavelength in the mode with the highest natural frequency. It means that if the length of the span is three times more than the span of interest, the number of the considered natural frequencies should be three times more than the previous simulation (cable with the normal span).

Considering a lengthy span omits the effects of the reflecting acceleration waves in the cable.

9.1 Existence of the droppers and the messenger cable

By using a lengthy span of the cable, the problem of the reflected waves appearing in the results is resolved. It is now time to add the messenger cable and the dropper into the model. The main targets in using the messenger cable and the droppers are actually removing the static deflection of the contact wire and improving the transferred electric current to the pantograph. In a real catenary system, the messenger cables are constrained to the Mast (Fig. 1) which has a very high vertical stiffness. In this situation the messenger cable can be considered as a clamp–clamp tensile beam. During installation, the length of the droppers is adjusted in a way that removes the sag in the contact wire. In the analytical model, the static force of the droppers should be calculated in a way that by applying the effect of the gravity and the calculated static force to the contact wire it remains sag free.

10 The length of the span for the modeling purposes

In a brief comparison, for the rail simulation purposes the length of the rail is an important parameter, since in reality the rail is very long and modeling of such lengths is impossible. For this reason, when modeling a rail a limited length of the rail is considered and the boundary conditions are included in such a way that the vibration waves are damped out with no reflections [26].

However, for the catenary systems the conditions are rather different. Contrary to the rail, the catenary overhead system is comprised of mechanical sections with limited lengths. These sections are mechanically (vibration wise) independent from each other. The length of these sections may vary from few 100 m to 2 km. A proper model for the simulation of the catenary system needs to also model its mechanical sections. In standard document EN50318 a mechanical section includes 10 spans of length 60 m each (600 m in total). This is introduced as a reference mechanical section in this document. Therefore, within this research a messenger cable with a length of 600 m is used for the modeling and its natural frequencies and mode shapes are obtained. Also, a contact wire with a length of 720 m (with an extra span at each end) is included in the modal analysis. The effect of the wave reflection within the first span of a mechanical section is negligible. However, the quality of wave clearly drops within the final spans of the mechanical section. The wave reflection within the latter spans of the mechanical section causes the deterioration of the mechanical contact.

11 Validation of the method

The software CatAna is designed to handle any number of sections for the catenary. However, validation of the model is by using ten sections. The specifics for the example models are also introduced. Within the software

Table 2 The specifics for the overhead catenary and pantograph systems that are used for the modeling

Parameter	Quantity	Parameter	Quantity	Parameter	Quantity
OCS					
Span length (m)	60	Mass of contact wire (kg/m)	1.35	Mass of messenger cable (kg/m)	1.07
Encumbrance (m)	1.2	Tension of contact wire (kN)	20	Tension of messenger cable (kN)	16
Encumbrance in the middle (m)	0	Contact wire flexural rigidity ($N\,m^2$)	195	Messenger cable flexural rigidity ($N\,m^2$)	131.17
Stagger (mm)	± 200	Dropper mass (kg/m)	0	Mass of clamp on contact wire (gr)	0
Number of spans	10	Mass of registration arm (gr)	400	Number of clamps per span	9
Clamp stiffness (kN/m)	10	Stiffness of registration arm (N/m)	340	Mass of clamp on messenger cable (gr)	0
The highest frequency considered (Hz): 60					
The number of modes considered for the contact wire: 680					
The number of modes considered for the messenger cable: 568					
Arrangement of droppers within the span (m)					
5 10.5 17 23.5 30 36.5 43 49.5 55					
Pantograph					
	Mass (kg)	Stiffness (N/m)	Damping (Ns/m)		
Blade	7.2	4200	10		
Body	15	50	90		
Stiffness of contact point (N/m) = 50,000					
Uplift force (N) = 100					
Pantograph speed (km/h) = 200					

CatAna the boundary conditions at the two ends of a mechanical section are introduced as two extra spans for the contact wire that are presented in Fig. 8. Such boundary conditions have the most similarity to the real overhead catenary systems.

The propagation and reflection of the waves is very vital to the modeling. This is also a reason for developing the analytical method of solution in this research. The reflection of waves and how they are trapped due to the nonlinear effect of the droppers is worked out and the results are presented.

11.1 Example case

The method of solution that is presented in this research in the form of software CatAna is used, as an example, with the set of data that is presented in Table 2 to model the slacking of the droppers. The outcome is presented in Fig. 11.

In Fig. 11, the left vertical axis is the relative displacement of the dropper and the right vertical axis is the dropper force. Until the compressive force within the dropper reaches $F_{\max}$, it behaves linearly with the relative displacement. Soon as the compressive forces go beyond $F_{\max}$, it then stays constant.

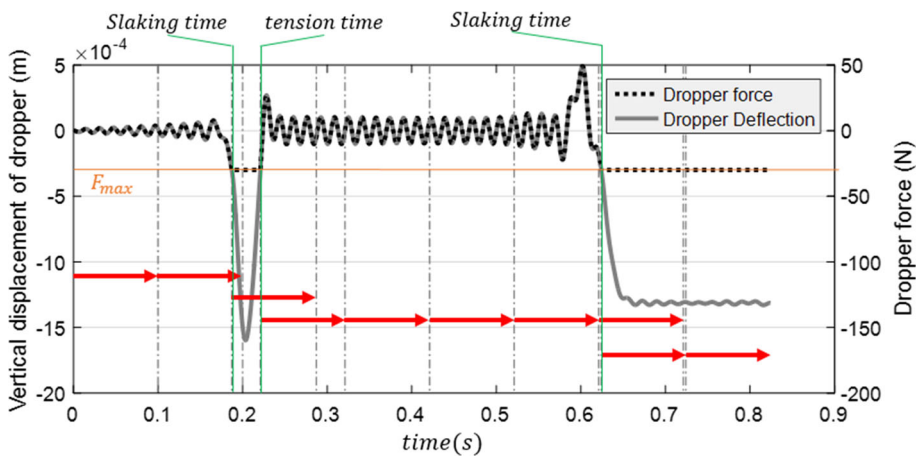

Fig. 11 The results of modeling the dropper slacking

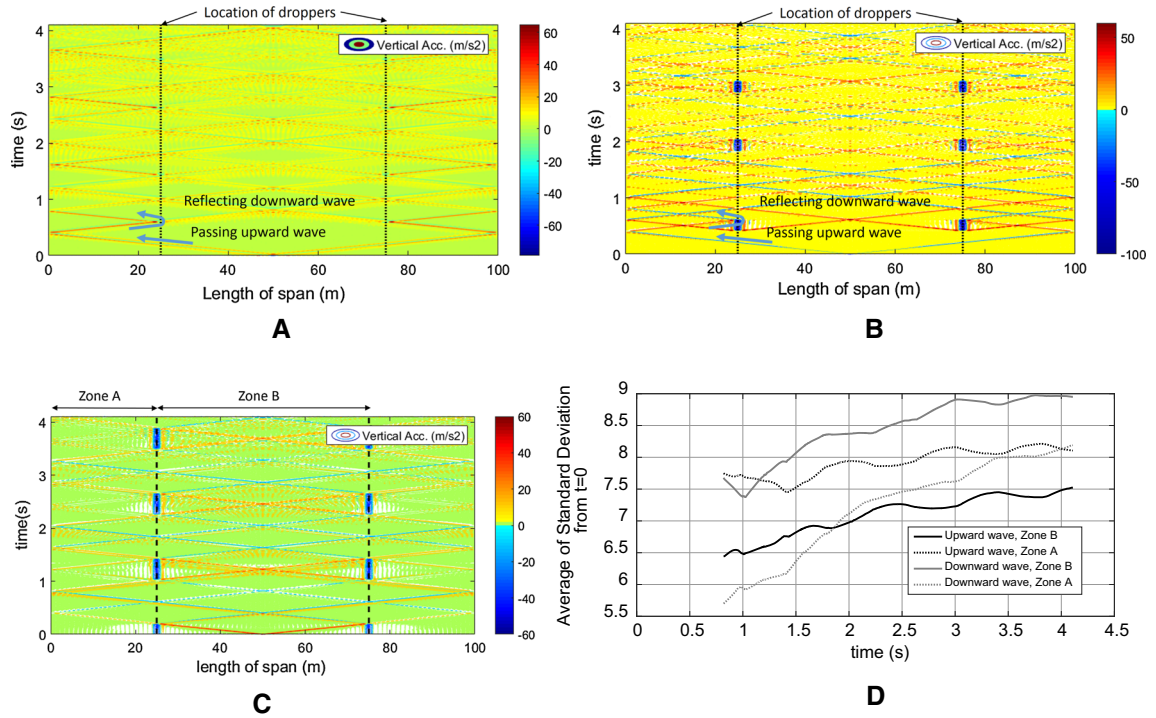

Fig. 12 **a** Acceleration of wire with nonlinear spring barrier (dropper) and initial displacement upward wave. **b** Acceleration of wire with nonlinear spring barrier and initial acceleration upward wave. **c** Acceleration of wire with nonlinear spring barrier and initial displacement downward wave. **d** The average of the standard deviation in different zones of cable for different cases

The red arrows in Fig. 11 indicate the time steps within the solution software. As soon as the force within any of the droppers exceeds $F_{\max}$, the stiffness of this component drops to zero. A constant downward force equal to $F_{\max}$ is applied in place of the dropper, and the new time step in calculations starts from this moment on. As soon as the estimated force within the dropper that is calculated based on its deflection tends to override $F_{\max}$, the stiffness of the dropper changes to its original value, the constant force is removed, and the new time step starts from this moment on. Therefore, by each slacking some simulation time will be wasted. The more the number of slacking, the more simulation time is required for modeling.

The effect of the presence and the location of the droppers (or the nonlinear springs) on the passing acceleration wave in the contact wire is simulated and is presented in Fig. 12.

In Fig. 12a–c, the horizontal axis represents the length of the span and the vertical axis represents the time. The vertical marker lines that are drawn at 25 m and 75 m represent the locations of the droppers. In Fig. 12a, an upward acceleration wave in the middle of the span acting as the initial condition at time ($t = 0.0$) is considered. In Fig. 12b the initial condition is an upward displacement wave in the middle of the span. In Fig. 12c the direction of the acceleration wave at the middle of the span is downward. In Fig. 12d the vertical axis presents the average of the standard deviation for the acceleration at different points along the span in zones A & B. Zones A&B are marked in Fig. 12c. The acceleration in the contact point is correlated with the contact force of the pantograph and catenary due to mass of the collector strip. Therefore, the results in Fig. 12d can define the quality of contact in zones A&B for the corresponding downward and upward waves.

The results in Fig. 12 indicate that for real cases, a dropper (that slacks in compression) in a catenary system has an interesting behavior when it faces upward waves. In fact, it acts as a rectifier because it lets an upward wave to pass through, but when the same wave reflects from the boundaries with a reverse figure (a downward wave), the dropper acts as a highly stiff barrier and reflects the wave. The wave then need to go to the boundary for a second time to have its figure reversed again to be able to pass through the dropper. This double passing of the waves happens between the boundaries and the closest dropper to the boundaries. This closest dropper is in the transient section (overlaps) of the contact wire, and the pantograph actually does not touch such section. The rectifying behavior of the dropper is the same for both acceleration and deflection waves, Fig. 12a, b. During such crossings and reflections, the energy of the wave dissipates in the contact wire and its boundary. Since all excited waves caused by a moving pantograph have upward direction, it is possible to claim that the

Table 3 Comparing the results from the analytical method of solution (CatAna) and those from EN 50318:2002

Speed (km/h)	250		300	
Model	Reference	CatAna	Reference	CatAna
Mean value (N)	110–120	118.48	110–120	117.83
Standard deviation (N)	26–31	27.26	32–40	30.41
Statistical maximum (N)	190–210	200.27	210-230	219.07
Statistical minimum (N)	20–40	36.69	− 5 to 20	16.59
Actual maximum (N)	175–210	206.76	190–225	212.15
Actual minimum (N)	50–70	53.88	30–55	21.48
Maximum uplift at support (mm)	40–55	50.33	55–65	58.52
Percentage of loss of contact (%)	0	0	0	0

slacking of the droppers reduces the acceleration disturbance in a zone of wire in contact with pantograph and moves this disturbance to zones of wire that never have connection with pantograph. Figure 12d compares the average of the standard deviation of each zone of wire under simulation. The average of the standard deviation is considered as the representative of the acceleration disturbance. It shows that for the downward wave, the acceleration disturbance in zone B is more than that in zone A. However, it is reversed for the upward wave. It seems that in real cases, the dropper in a catenary system can improve the contact quality close to the tension wheels that are located at the end of the mechanical sections.

11.2 Comparison with the standard document

The method of solution that is proposed in this research is validated by comparing it with the data that are available in standard document EN 50318: 2002. The reference model that is provided in the standard is used for demonstrating, and the contact force is calculated. Natural frequencies of the contact wire and the messenger cable up to 60Hz are included. The contact force is filtered by using a 20-Hz low-pass filter that is also compatible with the standard. The acceptable range for each parameter based on the standard recommendations, for the pantograph speed of travel at the two cases of 250 km/h and 300 km/h, is provided. The results are given in Table 3.

Also the procedure for calculating the droppers deal load and the contact wire and the messenger cable initial configurations, is compared with some other methods from reference [21]. It is concluded that the analytical method in this research is more accurate when compared with the finite elements and the finite differences methods.

11.3 Comparisons with other published results

Further validation of the results from this research is performed by comparing it with published data that are already available in the literature. Bruni et al. [27] introduced a reference model and asked ten research companies that were involved with the catenary pantograph dynamics to use their software programs and produce the modeling data. They then collected the results and compared them. This became a proper basis for the future modeling issues in this field. When comparing such results in addition to the dynamics of the pantograph moving under the overhead catenary system (OCS), its static parameters are also reported. The specifics for the OCS and the pantograph that are used for the modeling are extracted from the standard document EN50318 and are presented in Table 2. The results in the form of the static forces in the OCS droppers from ten software compared with the results from this research (CatAna) are presented in the following Table 4.

The information provided in [27] makes it clear that some of the design software assume that the contact wire support is a spring with low stiffness, while some other software programs consider such support as a fixed point in space. Keeping this in mind the software that is developed in this research (CatAna) is used to predict the results for both support cases. The results of the comparisons are provided in Fig. 13. The estimations for the contact wire static form from all ten software that are reported in [27] are within close proximity of each other. The results that are presented in Fig. 13 prove that the predictions by the analytical method from this research are very close to the other software results.

Since the droppers are located symmetrically within the span, the forces within the four last droppers are equal to the forces within the first four droppers. Considering the static balance of the contact wire and the fact

Table 4 A comparison for the dropper static force estimations by different software programs

Software	1st dropper x = 4.50	2nd dropper x = 10.25	3 rd dropper x = 16.0	4th dropper x = 21.75	5th dropper x = 27.5	Total dropper forces	Error %[a]
PrOSA	–	–	–	–	–	–	–
PantoCat	169.45	49.14	55.44	47.38	55.42	698.24	−7.213
SPOPS	198.10	53.06	54.24	54.17	54.15	773.29	2.760
CaPaSIM	161.98	52.14	51.90	51.98	51.69	687.69	−8.615
PCaDA	195.57	52.15	52.10	52.08	52.06	755.86	0.444
Gasen-do	171.32	50.09	55.89	47.80	55.84	706.04	−6.177
OSCAR	167.90	50.67	55.47	47.52	55.39	698.51	−7.177
TPL-PCRUN	162.61	52.43	56.20	48.55	56.20	695.78	−7.540
CANDY	155.56	52.24	56.58	48.01	54.80	679.58	−9.693
PACDIN	164.14	50.30	55.30	47.34	55.29	689.45	−8.381
δ[b]	14.067	1.255	1.614	2.442	1.527	30.621	–
CatAna	197.73	47.40	55.74	47.25	55.81	752.1	0.057

[a]The error in estimations is the difference between the sum of the dropper forces and the total weight of the cable and its accessories
[b]The standard deviation

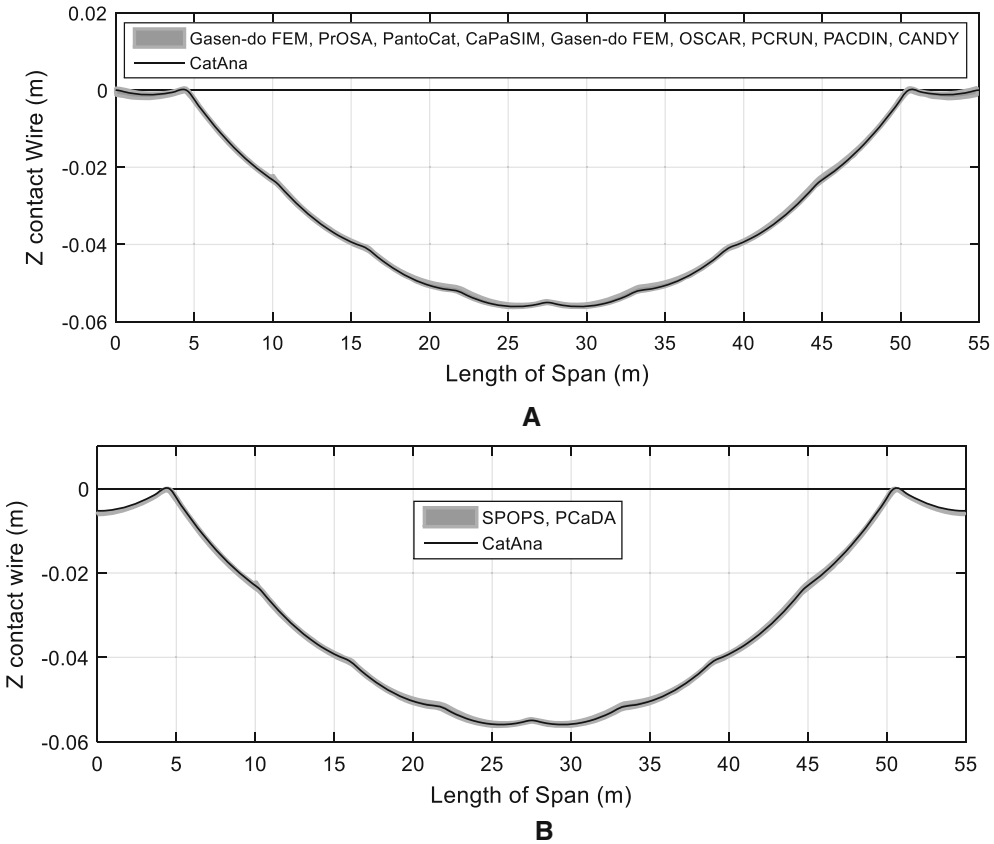

Fig. 13 A comparison between the analytical results from this research (CatAna) and the results from the finite elements method **a** while the contact wire supports are rigid, **b** while the contact wire supports are flexible

that the droppers have to tolerate the total weight of this wire, the total force within the droppers needs to be equal to the weight of the contact wire and its accessories. However, a little deviation from this total force in a span is logical and is presented in the last column in Table 4. It can be concluded that most of the available software programs that are based on the finite elements or finite differences methods generate considerable errors in their calculations. The sum of the forces applied to the contact wire by the droppers is not equal to the total weight of the wire and its accessories. On the contrary, the predictions in this research (CatAna) and the percentage of the error in calculations are much smaller. These errors in calculations in those software

programs come from the fact that the conditions of the support for the steady arm are not clear. As stated, some software programs consider it as a fixed point in space, while some others consider it as a spring support with low stiffness. Nonetheless, a portion of the weight of the contact wire and its accessories is tolerated by the steady arm and generates error in calculations. Such error is less affective in the analytical method and more so when the total number of modes within the calculations is increased.

12 Conclusions

This article presented a method of solution for calculating the interaction of the pantograph and the catenary through a modal approach. This is different from the other existing methods since they are based on the finite elements method. The low-order pantograph model is considered for the pantograph modeling. This model can simulate the wave crossing and reflection from different catenary barriers. Another advantage of this model is the consideration of the buckling force of the droppers in dropper slacking. Dropper slacking in contact wire is useful for reducing the acceleration in the contact point. Slacking of droppers lets the upward waves to pass but forces the downward waves to reflect. Therefore, it becomes possible to trap the acceleration or the displacement waves along the overlapping sections of the contact wire that the pantograph will actually never touch. A new analytical approach has been developed for estimating the initial configuration of the contact wire and the messenger cable that is more accurate than the FEM-based methods. Based on the proposed analytical method, a software is developed and the results are validated by comparing with EN 50318:2002.

Acknowledgements This research was supported by the office for "National Master Plan for High Speed Trains" at Iran University of Science and Technology. The authors are grateful for the support awarded.

Appendix A: Derivation of the stiffness, damping and mass matrices

$$\mathbf{M}\ddot{\mathbf{x}} + \mathbf{C}\dot{\mathbf{x}} + \mathbf{K}\mathbf{x} = \mathbf{f}$$

$$\mathbf{x} = \left[\, \mathbf{x_m}\ \mathbf{x_c}\ \mathbf{x_{s1}}\ \mathbf{x_{s2}}\ \cdots\ \mathbf{x_{p1}}\ \mathbf{x_{p2}}\ \cdots \right]^T$$

$$\mathbf{M} = \begin{bmatrix} \mathbf{M_m} & \mathbf{0} & \mathbf{0} & \mathbf{0} & \cdots & \mathbf{0} & \mathbf{0} & \mathbf{0} \\ \mathbf{0} & \mathbf{M_c} & \mathbf{0} & \mathbf{0} & \cdots & \mathbf{0} & \mathbf{0} & \mathbf{0} \\ \mathbf{0} & \mathbf{0} & \mathbf{M_{s1}} & \mathbf{0} & \cdots & \mathbf{0} & \mathbf{0} & \mathbf{0} \\ \mathbf{0} & \mathbf{0} & \mathbf{0} & \mathbf{M_{s2}} & \cdots & \mathbf{0} & \mathbf{0} & \mathbf{0} \\ \vdots & \vdots & \vdots & \vdots & \ddots & \vdots & \vdots & \vdots \\ \mathbf{0} & \mathbf{0} & \mathbf{0} & \mathbf{0} & \cdots & \mathbf{M_{p1}} & \mathbf{0} & \mathbf{0} \\ \mathbf{0} & \mathbf{0} & \mathbf{0} & \mathbf{0} & \cdots & \mathbf{0} & \mathbf{M_{p2}} & \mathbf{0} \\ \mathbf{0} & \mathbf{0} & \mathbf{0} & \mathbf{0} & \cdots & \mathbf{0} & \mathbf{0} & \ddots \end{bmatrix} \quad \mathbf{B} = \begin{bmatrix} \mathbf{f_{gm}} & \mathbf{f_{dm}} & \mathbf{0} \\ \mathbf{f_{gc}} & \mathbf{f_{dc}} & \mathbf{0} \\ \mathbf{f_{gs1}} & \mathbf{f_{ds1}} & \mathbf{0} \\ \mathbf{f_{gs2}} & \mathbf{f_{ds2}} & \mathbf{0} \\ \vdots & \vdots & \mathbf{0} \\ \mathbf{f_{gp1}} & \mathbf{0} & \begin{bmatrix} \mathbf{0} \\ \mathbf{1} \end{bmatrix} \\ \mathbf{f_{gp2}} & \mathbf{0} & \begin{bmatrix} \mathbf{0} \\ \mathbf{1} \end{bmatrix} \\ \vdots & \vdots & \vdots \end{bmatrix}$$

$$\mathbf{K} = \begin{bmatrix} \mathbf{K_m} & \mathbf{K_{mc}} & \mathbf{K_{ms1}} & \mathbf{K_{ms2}} & \cdots & \mathbf{0} & \mathbf{0} & \mathbf{0} \\ \mathbf{K_{cm}} & \mathbf{K_c} & \mathbf{K_{cs1}} & \mathbf{K_{cs2}} & \cdots & \left[\mathbf{k_{cp1}}\,(t)\ \mathbf{0}\right] & \left[\mathbf{k_{cp2}}\,(t)\ \mathbf{0}\right] & \cdots \\ \mathbf{K_{s1m}} & \mathbf{K_{s1c}} & \mathbf{K_{s1}} & \mathbf{0} & \cdots & \mathbf{0} & \mathbf{0} & \mathbf{0} \\ \mathbf{K_{s2m}} & \mathbf{K_{s2c}} & \mathbf{0} & \mathbf{K_{s2}} & \cdots & \mathbf{0} & \mathbf{0} & \mathbf{0} \\ \vdots & \vdots & \vdots & \vdots & \ddots & \vdots & \vdots & \vdots \\ \mathbf{0} & \begin{bmatrix} \mathbf{k_{p1c}}(t) \\ \mathbf{0} \end{bmatrix} & \mathbf{0} & \mathbf{0} & \cdots & \mathbf{K_{p1}} & \mathbf{0} & \mathbf{0} \\ \mathbf{0} & \begin{bmatrix} \mathbf{k_{p2c}}(t) \\ \mathbf{0} \end{bmatrix} & \mathbf{0} & \mathbf{0} & \cdots & \mathbf{0} & \mathbf{K_{p2}} & \mathbf{0} \\ \mathbf{0} & \vdots & \mathbf{0} & \mathbf{0} & \cdots & \mathbf{0} & \mathbf{0} & \ddots \end{bmatrix}$$

$$\mathbf{C}\text{-}\boldsymbol{K} \approx 0$$

$$\mathbf{c_{pic_{2\times nc}}}$$

should be calculated as follows.

Variable	Description	Variable	Description
$\mathbf{M}$	Mass matrix of whole system	m_{p1i}	Mass of collector strip of ith pantograph (Figure 5)
$\mathbf{C}$	Damping matrix of whole system	m_{p2i}	Second mass of ith pantograph (Figure 5)
$\mathbf{K}$	Stiffness matrix of whole system	$\mathbf{slk}$	Vector shows which dropper is on and which one is off due to slaking (0 or 1)
$\mathbf{f}$	Excitation factor	$\mathbf{slkm}$	Slaking vector of droppers which connects to messenger cable (0 or 1)
$\mathbf{x}$	Space state variable	$\mathbf{slks}$	Slaking vector of droppers which connects to stitch wires (0 or 1)
$\mathbf{x_m}$	Messenger cable Rayleigh-Ritz coefficient	$\mathbf{slksi}$	Slaking vector of droppers which connects to ith stitch wires (0 or 1)
$\mathbf{x_c}$	Contact wire Rayleigh–Ritz coefficient	$\mathbf{k_{dr}}$	Stiffness vector of droppers
$\mathbf{x_{si}}$	ith Stitch wire Rayleigh–Ritz coefficient	$\mathbf{k_{drm}}$	Stiffness vector of droppers which connects to messenger cable
$\mathbf{x_{pi}}$	ith Pantograph Rayleigh–Ritz coefficient	$\mathbf{k_{drs}}$	Stiffness vector of droppers which connects to stitch wires
$\mathbf{M_m}$	Mass matrix of messenger cable	$\mathbf{k_{drsi}}$	Stiffness vector of droppers which connects to ith stitch wire
$\mathbf{M_c}$	Mass matrix of contact wire	$\mathbf{k_{su}}$	Stiffness vector of messenger cable supports
$\mathbf{M_{si}}$	Mass matrix of ith stitch wire	$\mathbf{k_{stc}}$	Stiffness vector of stitch wire and messenger cable clamps
$\mathbf{M_{pi}}$	Mass matrix of ith pantograph	$\mathbf{k_{re}}$	Stiffness vector of registration arms
$\mathbf{K_m}$	Stiffness matrix of messenger cable	$\mathbf{k_{re}}$	Stiffness vector of contact point of droppers
$\mathbf{K_c}$	Stiffness matrix of contact wire	k_c	Stiffness of contact point (pantograph and catenary)
$\mathbf{K_{si}}$	Stiffness matrix of ith stitch wire	C_c	Damping of contact point (pantograph and catenary)
$\mathbf{K_p}$	Stiffness matrix of pantograph	k_{p1i}	Stiffness of collector strip of ith pantograph (Figure 5)
$\mathbf{K_{mc}}$	Relative stiffness matrix between messenger cable and contact wire	k_{p2i}	Second stiffness of ith pantograph (Figure 5)
$\mathbf{K_{msi}}$	Relative stiffness matrix between messenger cable and ith stitch wire	$\boldsymbol{c_{dr}}$	Damping vector of droppers
$\mathbf{K_{csi}}$	Relative stiffness matrix between contact wire and ith stitch wire	$\boldsymbol{c_{drm}}$	Damping vector of droppers which connects to messenger cable
$\mathbf{K_{cpi}}$	Relative stiffness matrix between contact wire and ith pantograph	$\mathbf{c_{drs}}$	Damping vector of droppers which connects to stitch wires
αm	Mass coefficient of messenger cable	$\mathbf{c_{drsi}}$	Damping vector of droppers which connects to ith stitch wire
αc	Mass coefficient of contact wire	$\mathbf{c_{su}}$	Damping vector of messenger cable supports
αs	Mass coefficient of stitch wire	$\mathbf{c_{stc}}$	Damping vector of stitch wire and messenger cable clamps

Variable	Description	Variable	Description
m_{ucdr}	Mass of upper clamp of dropper	$\mathbf{c_{re}}$	Damping vector of registration arms
m_{lcdr}	Mass of lower clamp of dropper	$\mathbf{c_{re}}$	Damping vector of contact point of droppers
m_{cst}	Mass of connection clamp of stitch wire and messenger cable	c_{p1i}	Damping of collector strip of ith pantograph (Figure 5)
em_{re}	Equivalent mass of registration arm	c_{p2i}	Second Damping of ith pantograph (Figure 5)
x_{drm}	Location of droppers in messenger cable	$\mathbf{\Omega_m^2}$	Diagonal matrix of square of messenger cable natural frequencies.
x_{drc}	Location of droppers in contact wire	$\mathbf{\Omega}_c^2$	Diagonal matrix of square of contact wire natural frequencies
x_{drs}	Location of droppers in stitch wire	$\mathbf{\Omega}_s^2$	Diagonal matrix of square of stitch wire natural frequencies.
x_{drcsi}	Location of droppers of ith stitch wire in contact wire	$\mathbf{Z_m^2}$	Diagonal matrix of square of messenger cable natural frequencies.
x_{rem}	Location of registration arm in messenger cable	$\mathbf{Z_c^2}$	Diagonal matrix of square of contact wire natural frequencies.
x_{rec}	Location of registration arm in contact wire	$\mathbf{Z_s^2}$	Diagonal matrix of square of stitch wire natural frequencies
x_{stcm}	Location of stitch wires connection on messenger cable	$\mathbf{u_{3\times 1}}$	Input vector of system including weight, dead load of droppers and uplift force
x_{stcmi}	Location of ith stitch wire connection on messenger cable	F_{uplift}	Uplift force which is applied to pantograph
x_{stcs}	Location of stitch wire connection on stitch wire $(l_{\text{st}}, 0)$.	$\mathbf{f_{gm}}$	Gravity force on messenger cable
$\mathbf{x_{pac}}(t)$	Location vector of pantographs on contact wire	$\mathbf{f_{gc}}$	Gravity force on contact wire
$x_{\text{paci}}(t)$	Location of ith pantograph on contact wire	$\mathbf{f_{gsi}}$	Gravity force on ith Stitch wire
$\mathbf{\Phi m(x, n)}$	Mode shape matrix of messenger cable in n mode and x location	$\mathbf{f_{gpi}}$	Gravity force on ith pantograph
$\boldsymbol{\Phi s(x,n)}$	Mode shape matrix of stitch wire in n mode and x location	$\mathbf{f_{dm}}$	Dead loads of droppers on messenger cable
$\mathbf{\Phi c(x, n)}$	Mode shape matrix of contact wire in n mode and x location	$\mathbf{f_{dc}}$	Dead loads of droppers on contact wire
$\mathbf{\acute{\Phi} c(x, n)}$	Gradient of mode shape matrix of contact wire in n mode and x location	$\mathbf{f_{dsi}}$	Dead loads of droppers on stitch wire
nm	Number of considered mode shape for messenger cable	ρA_{m}	Mass per unit length of messenger cable
nc	Number of considered mode shape for contact wire	ρA_{c}	Mass per unit length of contact wire
ns	Number of considered mode shape for stitch wire	ρA_{s}	Mass per unit length of stitch wire
nsp	Number of spans	$F0_{\text{drm}}$	Dead load of droppers connected to messenger cable
$ndrm$	Number of connected dropper to messenger cable	$F0_{\text{drs}}$	Dead load of droppers connected to stitch wire
$ndrsi$	Number of connected dropper to ith stitch wire	Δ_{m}	The initial location of dropper clamps on messenger cable
ndr	Number of dropper	Δ_{cm}	The initial location of dropper clamps on contact wire (droppers connected to messenger cable)
l_{st}	Length of stitch wire	Δ_{cs}	The initial location of dropper clamps on contact wire (droppers connected to stitch wire)
		Δ_{s}	The initial location of dropper clamps on stitch wire

Parameter	Description
$\mathbf{M_{m_{nm\times nm}}}$	$(\alpha\mathbf{m_{nm\times 1}}.m_{ucdr}\mathbf{I_{1\times nm}})\cdot\left(\mathbf{\Phi m}(\mathbf{x_{drm}},\mathbf{n})_{\mathbf{nm\times ndrm}}\left(\mathbf{\Phi m}(\mathbf{x_{drm}},\mathbf{n})_{\mathbf{nm\times ndrm}}\right)^{\mathbf{T}}\right)+$ $(\alpha\mathbf{m_{nm\times 1}}.m_{cst}\mathbf{I_{1\times nm}})\cdot\left(\mathbf{\Phi m}(\mathbf{x_{stcm}},\mathbf{n})_{\mathbf{nm\times 2(nsp+1)}}\left(\mathbf{\Phi m}(\mathbf{x_{stcm}},\mathbf{n})_{\mathbf{nm\times 2(nsp+1)}}\right)^{\mathbf{T}}\right)+\mathbf{I_{nm\times nm}}$
$\mathbf{M_{c_{nc\times nc}}}$	$(\alpha\mathbf{c_{nc\times 1}}.m_{lcdr}\times\mathbf{I_{1\times nc}})\cdot\left(\mathbf{\Phi c}(\mathbf{x_{dr}},\mathbf{n})_{\mathbf{nc\times ndr}}\left(\mathbf{\Phi c}(\mathbf{x_{dr}},\mathbf{n})_{\mathbf{nc\times ndr}}\right)^{\mathbf{T}}\right)+(\alpha\mathbf{c_{nc\times 1}}.\mathbf{em_{re}I_{1\times nc}})\cdot\left(\mathbf{\Phi c}(\mathbf{x_{rec}},\mathbf{n})_{\mathbf{nc\times nsp+1}}\left(\mathbf{\Phi c}(\mathbf{x_{rec}},\mathbf{n})_{\mathbf{nc\times nsp+1}}\right)^{\mathbf{T}}\right)+\mathbf{I_{nc\times nc}}$
$\mathbf{M_{si_{ns\times ns}}}$	$(\alpha\mathbf{s_{ns\times 1}}.\mathbf{m_{ucdr}I_{1\times ns}})\cdot\left(\mathbf{\Phi s}(\mathbf{x_{drs}},\mathbf{n})_{\mathbf{ns\times ndrs}}\left(\mathbf{\Phi s}(\mathbf{x_{drs}},\mathbf{n})_{\mathbf{ns\times ndrs}}\right)^{\mathbf{T}}\right)+(\alpha\mathbf{s_{ns\times 1}}.\mathbf{m_{cst}I_{1\times ns}})\cdot\left(\mathbf{\Phi s}(\mathbf{x_{stcs}},\mathbf{n})_{\mathbf{ns\times 2}}\left(\mathbf{\Phi s}(\mathbf{x_{stcs}},\mathbf{n})_{\mathbf{ns\times 2}}\right)^{\mathbf{T}}\right)+\mathbf{I_{ns\times ns}}$
$\mathbf{M_{pi_{2\times 2}}}$	$\begin{bmatrix}\mathbf{m_{p1i}} & \mathbf{0}\\ \mathbf{0} & \mathbf{m_{p2i}}\end{bmatrix}$
$\mathbf{K_{m_{nm\times nm}}}$	$\left((\alpha\mathbf{m_{nm\times 1}}(\mathbf{slkm}.\mathbf{k_{drm}}))_{\mathbf{nm\times ndrm}}.\mathbf{\Phi m}(\mathbf{x_{drm}},\mathbf{n})_{\mathbf{nm\times ndrm}}\right)\left(\mathbf{\Phi m}(\mathbf{x_{drm}},\mathbf{n})_{\mathbf{nm\times ndrm}}\right)^{\mathbf{T}}$ $+\left((\alpha\mathbf{m_{nm\times 1}}.\mathbf{k_{stc}})_{\mathbf{nm\times 2(nsp+1)}}.\mathbf{\Phi m}(\mathbf{x_{stcm}},\mathbf{n})_{\mathbf{nm\times 2(nsp+1)}}\right)\left(\mathbf{\Phi m}(\mathbf{x_{stcm}},\mathbf{n})_{\mathbf{nm\times 2(nsp+1)}}\right)^{\mathbf{T}}$ $+\left((\alpha\mathbf{m_{nm\times 1}}.\mathbf{k_{su}})_{\mathbf{nm\times nsp+1}}.\mathbf{\Phi m}(\mathbf{x_{rem}},\mathbf{n})_{\mathbf{nm\times nsp+1}}\right)\left(\mathbf{\Phi m}(\mathbf{x_{rem}},\mathbf{n})_{\mathbf{nm\times nsp+1}}\right)^{\mathbf{T}}+\omega^2_{\mathbf{m_{nm\times nm}}}$
$\mathbf{K_{c_{nc\times nc}}}$	$\left((\alpha\mathbf{c_{nc\times 1}}(\mathbf{slk}.\mathbf{k_{dr}}))_{\mathbf{nc\times ndr}}.\mathbf{\Phi c}(\mathbf{x_{drc}},\mathbf{n})_{\mathbf{nc\times ndr}}\right)\left(\mathbf{\Phi c}(\mathbf{x_{drc}},\mathbf{n})_{\mathbf{nc\times ndr}}\right)^{\mathbf{T}}+\left((\alpha\mathbf{c_{nc\times 1}}.\mathbf{k_{re}})_{\mathbf{nc\times nsp+1}}.\mathbf{\Phi c}(\mathbf{x_{rec}},\mathbf{n})_{\mathbf{nc\times nsp+1}}\right)\left(\mathbf{\Phi c}(\mathbf{x_{rec}},\mathbf{n})_{\mathbf{nc\times nsp+1}}\right)^{\mathbf{T}}$ $+\left((\alpha\mathbf{c_{nm\times 1}}.\mathbf{k_c})_{\mathbf{nc\times npan}}.\mathbf{\Phi c}\left(\mathbf{x_{pac}}(t),\mathbf{n}\right)_{\mathbf{nc\times npan}}\right)\left(\mathbf{\Phi c}\left(\mathbf{x_{pan}}(t),\mathbf{n}\right)_{\mathbf{nc\times npan}}\right)^{\mathbf{T}}+\Omega^2_{\mathbf{c_{nc\times nc}}}$
$\mathbf{K_{si_{ns\times ns}}}$	$\left((\alpha\mathbf{s_{ns\times 1}}(\mathbf{slksi}.\mathbf{k_{drsi}}))_{\mathbf{ns\times ndrsi}}.\mathbf{\Phi s}(\mathbf{x_{drs}},\mathbf{n})_{\mathbf{ns\times ndrsi}}\right)\left(\mathbf{\Phi s}(\mathbf{x_{drs}},\mathbf{n})_{\mathbf{ns\times ndrsi}}\right)^{\mathbf{T}}+\left((\alpha\mathbf{s_{ns\times 1}}.\mathbf{k_{stc}})_{\mathbf{ns\times 2}}.\mathbf{\Phi s}(\mathbf{x_{stcs}},\mathbf{n})_{\mathbf{ns\times 2}}\right)\left(\mathbf{\Phi s}(\mathbf{x_{stcs}},\mathbf{n})_{\mathbf{ns\times 2}}\right)^{\mathbf{T}}+\Omega^2_{\mathbf{s_{ns\times ns}}}$
$\mathbf{K_{mc_{nm\times nc}}}$	$\left((\alpha\mathbf{m_{nm\times 1}}(\mathbf{slkm}.\mathbf{k_{drm}}))_{\mathbf{nm\times ndrm}}.\mathbf{\Phi m}(\mathbf{x_{drm}},\mathbf{n})_{\mathbf{nm\times ndrm}}\right)\left(\mathbf{\Phi c}(\mathbf{x_{drm}},\mathbf{n})_{\mathbf{nc\times ndrm}}\right)^{\mathbf{T}}$
$\mathbf{K_{cm_{nc\times nm}}}$	$\left((\alpha\mathbf{c_{nc\times 1}}(\mathbf{slkm}.\mathbf{k_{drm}}))_{\mathbf{nc\times ndrm}}.\mathbf{\Phi c}(\mathbf{x_{drm}},\mathbf{n})_{\mathbf{nc\times ndrm}}\right)\left(\mathbf{\Phi m}(\mathbf{x_{drm}},\mathbf{n})_{\mathbf{nm\times ndrm}}\right)^{\mathbf{T}}$
$\mathbf{K_{msi}K_{msi_{nm\times nsi}}}$	$\left((\alpha\mathbf{m_{nm\times 1}}\mathbf{k_{stc}})_{\mathbf{nm\times 2}}.\mathbf{\Phi m}(\mathbf{x_{stcmi}},\mathbf{n})_{\mathbf{nm\times 2}}\right)\left(\mathbf{\Phi s}(\mathbf{x_{stcs}},\mathbf{n})_{\mathbf{ns\times 2}}\right)^{\mathbf{T}}$
$\mathbf{K_{sic_{ns\times nc}}}$	$\left((\alpha\mathbf{s_{ns\times 1}}\mathbf{k_{stc}})_{\mathbf{ns\times 2}}.\mathbf{\Phi s}(\mathbf{x_{stcs}},\mathbf{n})_{\mathbf{ns\times 2}}\right)\left(\mathbf{\Phi m}(\mathbf{x_{stcmi}},\mathbf{n})_{\mathbf{ns\times 2}}\right)^{\mathbf{T}}$
$\mathbf{K_{csi_{nc\times ns}}}$	$\left((\alpha\mathbf{c_{nc\times 1}}(\mathbf{slksi}.\mathbf{k_{drsi}}))_{\mathbf{nc\times ndrsi}}.\mathbf{\Phi c}(\mathbf{x_{drcsi}},\mathbf{n})_{\mathbf{nc\times ndrsi}}\right)\left(\mathbf{\Phi s}(\mathbf{x_{drs}},\mathbf{n})_{\mathbf{ns\times ndrsi}}\right)^{\mathbf{T}}$
$\mathbf{K_{sic_{ns\times nc}}}$	$\left((\alpha\mathbf{s_{ns\times 1}}(\mathbf{slksi}.\mathbf{k_{drsi}}))_{\mathbf{ns\times ndrsi}}.\mathbf{\Phi s}(\mathbf{x_{drs}},\mathbf{n})_{\mathbf{ns\times ndrsi}}\right)\left(\mathbf{\Phi c}(\mathbf{x_{drcsi}},\mathbf{n})_{\mathbf{nc\times ndrsi}}\right)^{\mathbf{T}}$
$\mathbf{K_{cpi_{nc\times 2}}}$	$-\left(\vec{\alpha}\mathbf{c_{nc\times 1}}.k_c\right)_{\mathbf{nc\times 1}}.\varphi\mathbf{c}\left(\mathbf{x_{paci}}(t),\mathbf{n}\right)_{\mathbf{nc\times 1}}$
$\mathbf{K_{pic_{2\times nc}}}$	$-k_c.\left(\mathbf{\Phi c}\left(\mathbf{x_{paci}}(\mathbf{t}),\mathbf{n}\right)_{\mathbf{nc\times 1}}\right)^{\mathbf{T}}-V_pC_c.\left(\dot{\mathbf{\Phi}}\mathbf{c}\left(\mathbf{x_{paci}}(t),\mathbf{n}\right)_{\mathbf{nc\times 1}}\right)^{\mathbf{T}}$
$\mathbf{C_{pic_{2\times nc}}}$	$-c_c.\left(\left[\mathbf{\Phi c}\left(\mathbf{x_{paci}}(t),\mathbf{n}\right)\right]_{\mathbf{nc\times 1}}\right)^{\mathbf{T}}$
$\mathbf{K_{pi_{2\times 2}}}$	$\begin{bmatrix}k_{p1i}+k_c & -k_{p1i}\\ -k_{p1i} & k_{p1i}+k_{p2i}\end{bmatrix}$
$\mathbf{u_{3\times 1}}$	$\left[\mathrm{g}\ 1\ f_{uplift}\right]^{\mathbf{T}}$
f_{gm}	$-\rho A_m.\boldsymbol{\alpha}\mathbf{m}_{nm\times 1}.\left(\int\mathbf{\Phi m}\,(x,n)dx\right)_{nm\times 1}-(m_{ucdr}.\boldsymbol{\alpha}\mathbf{m}_{nm\times 1})\cdot\left(\mathbf{I}_{1\times ndrm}\left([\mathbf{\Phi m}(\mathbf{x_{drm}},\mathbf{n})]_{\mathbf{nm\times ndrm}}\right)^{T}\right)$
$\mathbf{f_{dm}}$	$\alpha\mathbf{m_{nm\times 1}}.((\mathbf{k_{drm}}.(\Delta_{\mathbf{m}}-\Delta_{\mathbf{cm}})-\mathbf{f0_{drm}})_{\mathbf{1\times ndrm}}\times\left(\mathbf{\Phi m}(\mathbf{x_{drm}},\mathbf{n})_{\mathbf{nm\times ndrm}}\right)^{\mathbf{T}})^{\mathbf{T}}$
$\mathbf{f_{gc}}$	$-\rho\mathbf{A_c}.\boldsymbol{\alpha}\mathbf{c_{nc\times 1}}.\left(\int\mathbf{\Phi c}\,(\mathbf{x},\mathbf{n})\mathbf{dx}\right)_{\mathbf{nc\times 1}}-(m_{lcdr}.\boldsymbol{\alpha}\mathbf{c_{nc\times 1}})\cdot\left(\mathbf{I_{1\times ndr}}\times\left(\mathbf{\Phi c}(\mathbf{x_{drc}},\mathbf{n})_{\mathbf{nc\times ndr}}\right)^{\mathbf{T}}\right)$
$\mathbf{f_{dc}}$	$-\alpha\mathbf{c_{nc\times 1}}.((\mathbf{k_{drm}}.(\Delta_{\mathbf{m}}-\Delta_{\mathbf{cm}})-\mathbf{f0_{drm}})_{\mathbf{1\times ndrm}}\times\left(\mathbf{\Phi c}(\mathbf{x_{drm}},\mathbf{n})_{\mathbf{nc\times ndrm}}\right)^{\mathbf{T}})^{\mathbf{T}}-\alpha\mathbf{c_{nc\times 1}}.((\mathbf{k_{drs}}.(\Delta_{\mathbf{s}}-\Delta_{\mathbf{cs}})-\mathbf{f0_{drs}})_{\mathbf{1\times ndrs}}\times\left(\mathbf{\Phi c}(\mathbf{x_{drs}},\mathbf{n})_{\mathbf{nc\times ndrs}}\right)^{\mathbf{T}})^{\mathbf{T}}$
$\mathbf{f_{gsi}}$	$-\rho A_s.\boldsymbol{\alpha}\mathbf{s_{ns\times 1}}.\left(\int[\mathbf{\Phi s}\,(\mathbf{x},\mathbf{n})]\,\mathbf{dx}\right)_{\mathbf{ns\times 1}}-(\mathbf{m_{ucdr}}.\boldsymbol{\alpha}\mathbf{s_{ns\times 1}})\cdot\left(\mathbf{I_{1\times ndrs}}\times\left(\mathbf{\Phi s}(\mathbf{x_{drs}},\mathbf{n})_{\mathbf{ns\times ndrs}}\right)^{\mathbf{T}}\right)$
$\mathbf{f_{ds}}$	$\alpha\mathbf{s_{ns\times 1}}.((\mathbf{k_{drs}}.(\Delta_{\mathbf{s}}-\Delta_{\mathbf{cs}})-\mathbf{f0_{drs}})_{\mathbf{1\times ndrs}}\times\left(\mathbf{\Phi s}(\mathbf{x_{drs}},\mathbf{n})_{\mathbf{ns\times ndrs}}\right)^{\mathbf{T}})^{\mathbf{T}}$
$\mathbf{f_{gpi}}$	$\left[\mathbf{m_{p1i}}\ \mathbf{m_{p2i}}\right]^{\mathbf{T}}$

References

1. EN, B.: Technical criteria for the interaction between pantograph and overhead line. In: EN 50367 (2012)
2. Zhang, W., Zou, D., Tan, M., Zhou, N., Li, R., Mei, G.: Review of pantograph and catenary interaction. Front. Mech. Eng. **13**(2), 311–322 (2018)
3. Kulkami, S., Pappalardo, C.M., Shabana, A.A.: Pantograph/catenary contact formulations. J. Vib. Acoust. **139**(1), 52 (2017)
4. Van Vo, O., Massat, J.-P., Balmes, E.: Waves, modes and properties with a major impact on dynamic pantograph–catenary interaction. J. Sound Vib. **402**, 51–69 (2017)
5. Sorrentino, S., Anastasio, D., Fasana, A., Marchesiello, S.: Distributed parameter and finite element models for wave propagation in railway contact lines. J. Sound Vib. **410**, 1–18 (2017)
6. Song, Y., Ouyang, H., Liu, Z., Mei, G., Wang, H., Xiaobing, L.: Active control of contact force for high-speed railway pantograph–catenary based on multi-body pantograph model. Mech. Mach. Theory **115**, 35–59 (2017)
7. Zhou, N., Lv, Q., Yang, Y., Zhang, W.: TPL-PCRUN statement of methods. Veh. Syst. Dyn. **53**, 380–391 (2015)
8. Tur, M., Baeza, L., Fuenmayor, F., García, E.: PACDIN statement of methods. Veh. Syst. Dyn. **53**, 402–411 (2015)
9. Sánchez-Rebollo, C., Carnicero, A., Jiménez-Octavio, J.: CANDY statement of methods. Veh. Syst. Dyn. **53**, 392–401 (2015)
10. Jönsson, P.-A., Stichel, S., Nilsson, C.: CaPaSIM statement of methods. Veh. Syst. Dyn. **53**, 341–346 (2015)
11. Ikeda, M.: 'Gasen-do FE'statement of methods. Veh. Syst. Dyn. **53**, 357–369 (2015)
12. Finner, L., Poetsch, G., Sarnes, B., Kolbe, M.: Program for catenary–pantograph analysis, PrOSA statement of methods and validation according EN 50318. Veh. Syst. Dyn. Int. J. Veh. Mech. Mobil. **53**(3), 305–313 (2015)
13. Collina, A., Bruni, S., Facchinetti, A., Zuin, A.: PCaDA statement of methods. Veh. Syst. Dyn. **53**, 347–356 (2015)
14. Cho, Y.H.: SPOPS statement of methods. Veh. Syst. Dyn. **53**, 329–340 (2015)
15. Ambrósio, J., Pombo, J., Antunes, P., Pereira, M.: PantoCat statement of method. Veh. Syst. Dyn. **53**, 314–328 (2015)
16. Kia, S. H., Bartolini, F., Mpanda-Mabwe, A., Ceschi, R.: Pantograph–catenary interaction model comparison. In: IECON 2010-36th Annual Conference on IEEE Industrial Electronics Society, pp. 1584–1589 (2010)
17. Leissa, A.W., Qatu, M.S.: Vibrations of Continuous Systems. McGraw-Hill, New York (2011)
18. Zhou, N., Lv, Q., Yang, Y., Zhang, W.: TPL-PCRUN statement of methods. Veh. Syst. Dyn. Int. J. Veh. Mech. Mobil. **53**(3), 380–391 (2015). https://doi.org/10.1080/00423114.2014.982136
19. Kargarnovin, M.H., Younesian, D., Thompson, D., Jones, C.: Ride comfort of high speed trains travelling over railway bridges. Veh. Syst. Dyn. **43**(3), 173–197 (2005)
20. Dormand, J.R., Prince, P.J.: A family of embedded Runge–Kutta formulae. J. Comput. Appl. Math. **6**, 19–26 (1980)
21. Vesali, F., Molatefi, H., Rezvani, M.A.: Using new analytical algorithm to study the effect of temperature variations on static shape of contact wire of OCS. J. Vibroeng. **18**, 2061–2073 (2016)
22. Ambrósio, J., Pombo, J., Pereira, M., Antunes, P., Mósca, A.: Recent developments in pantograph–catenary interaction modelling and analysis. Int. J. Railw. Technol. **1**, 249–278 (2012)
23. Lindberg, H.E.: Little book of dynamic buckling. In: LCE Science/Software (2003)
24. Kuzkin, V.A.: Structural model for the dynamic buckling of a column under constant rate compression. arXiv preprint arXiv:1506.00427 (2015)
25. Kia, S.H., Bartolini, F., Mpanda-Mabwe, A.: Pantograph–catenary interaction model comparison. In: IECON 2010-36th Annual Conference on IEEE Industrial Electronics Society, IEEE (2010)
26. Manchem, L.D., Srinivasan, M.N., Zhou, J.: Analytical modeling of residual stress in railroad rails using critically refracted longitudinal ultrasonic waves with COMSOL multiphysics module. In: Srinivasan, A, Zhou, J. (eds.), International Mechanical Engineering Congress and Exposition, Canada. No. 9 (2014)
27. Bruni, S., Ambrosio, J., Carnicero, A., Cho, Y.H., Finner, L., Ikeda, M., Kwon, S.Y., Massat, J.-P., Stichel, S., Tur, M., Zhang, W.: The results of the pantograph–catenary interaction benchmark. Veh. Syst. Dyn. Int. J. Veh. Mech. Mobil. **53**(3), 412–435 (2015)